PART I

RODS AND ROPES

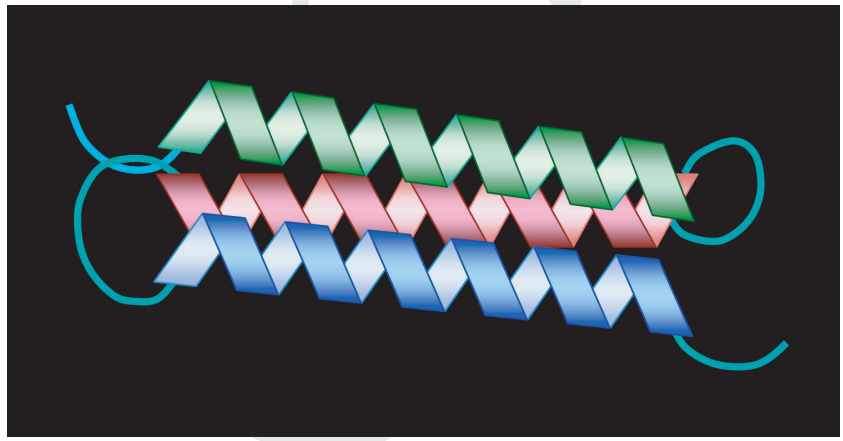

3 Polymers

The structural elements of the cell can be broadly classified as filaments or sheets, where by the term filament, we mean a string-like object whose length is much greater than its width. Some filaments, such as DNA, function as mechanically independent units, but most structural filaments in the cell are linked to form two- or three-dimensional networks. As seen on the cellular length scale of a micron, individual filaments may be relatively straight or highly convoluted, reflecting, in part, their resistance to bending. Part I of this book concentrates on the mechanical properties of biofilaments: Chapter 3 covers the bending and stretching of simple filaments while Chapter 4 explores the structure and torsion resistance of complex filaments. The two chapters making up the remainder of Part I consider how filaments are knitted together to form networks, perhaps closely associated with a membrane as a two-dimensional web (Chapter 5) or perhaps extending though the three-dimensional volume of the cell (Chapter 6).

3.1 Polymers and simple biofilaments

At the molecular level, the cell's ropes and rods are composed of linear polymers, individual monomeric units that are linked together as an unbranched chain. The monomers need not be identical, and may themselves be constructed of more elementary chemical units. For example, the monomeric unit of DNA and RNA is a troika of phosphate, sugar and organic base, with the phosphate and sugar units alternating along the backbone of the polymer (see Chapter 4 and Appendix B). However, the monomers are not completely identical because the base may vary from one monomer to the next. The double helix of DNA contains two such sugar–base–phosphate strands, with a length along the helix of 0.34 nm per pair of organic bases, and a corresponding molecular mass per unit length of about 1.9 kDa/nm (Saenger, 1984).

The principal components of the cytoskeleton – actin, intermediate filaments and microtubules – are themselves composite structures made from protein subunits, each of which is a linear chain hundreds of amino acids long. In addition, some cells contain fine strings of the protein spectrin,

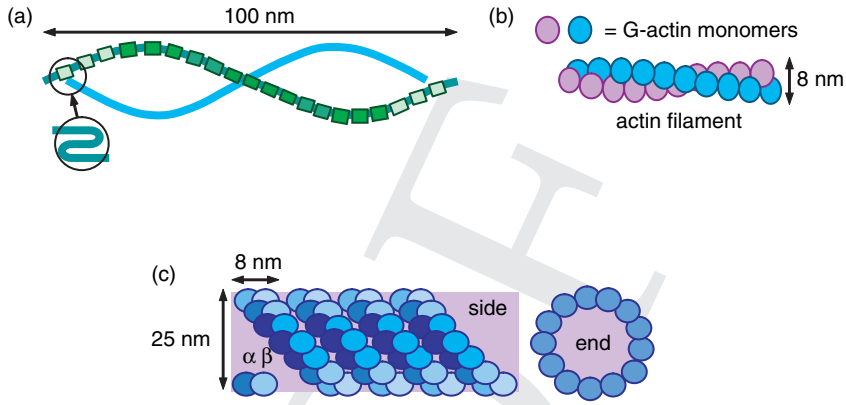

Fig. 3.1 (a) Two spectrin chains intertwine in a filament, where the boxes represent regions in which the protein chain has folded back on itself (as in the inset). The two strings are stretched and separated for clarity. (b) Monomers of G-actin associate to form a filament of F-actin, which superficially appears like two intertwined strands. (c) Microtubules usually contain 13 protofilaments, whose elementary unit is an 8 nm long dimer of the proteins α and β tubulin. Both side and end views of the cylinder are shown.

whose structure we discuss first before considering the thicker filaments of the cytoskeleton. As organized in the human erythrocyte, two pairs of chains, each pair containing two intertwined and inequivalent strings of spectrin (called α and β), are joined end-to-end to form a filament about 200 nm in contour length. The α and β chains have molecular masses of 230 and 220 kDa, respectively, giving a mass per unit length along the tetramer of 4.5 kDa/nm. An individual chain folds back on itself repeatedly like a Z, so that each monomer is a series of 19 or 20 relatively rigid barrels 106 amino acid residues long, as illustrated in Fig. 3.1(a).

Forming somewhat thicker filaments than spectrin, the protein actin is present in many different cell types and plays a variety of roles in the cytoskeleton. The elementary actin building block is the protein G-actin ("G" for globular), a single chain of approximately 375 amino acids having a molecular mass of 42 kDa. G-actin units can assemble into a long string called F-actin ("F" for filamentous), which, as illustrated in Fig. 3.1(b), has the superficial appearance of two strands forming a coil, although the strands are not, in fact, independently stable. The filament has a width of about 8 nm and a mass per unit length of 16 kDa/nm. Typical actin monomer concentrations in the cell are 1–5 mg/ml; as a benchmark, a concentration of 1 mg/ml is 24 μM for a molecular mass of 42 kDa.

The thickest individual filaments are composed of the protein tubulin, present as a heterodimer of α-tubulin and β-tubulin, each with a molecular mass of about 50 kDa. Pairs of α- and β-tubulin form a unit 8 nm in length, and these units can assemble α to β successively into a hollow

microtubule consisting of 13 linear protofilaments (in almost all cells), as shown in Fig. 3.1(c). The overall molecular mass per unit length of a microtubule is about 160 kDa/nm, ten times that of actin. Tubulin is present at concentrations of a few milligrams per milliliter in a common cell; given a molecular mass of 100 kDa for a tubulin dimer, a concentration of 1 mg/ml corresponds to 10 μM.

Intermediate filaments lie in diameter between microtubules and F-actin. As will be described further in Chapter 4, intermediate filaments are composed of individual strands with helical shapes that are bundled together to form a composite structure with 32 strands. Depending on the type, an intermediate filament has a roughly cylindrical shape about 10 nm in diameter and a mass per unit length of about 35 kDa/nm, with some variation. Desmin and vimentin are somewhat higher at 40–60 kDa/nm (Herrmann *et al*., 1999); neurofilaments are also observed to lie in the 50 kDa/nm range (Heins *et al*., 1993). Further examples of composite filaments are collagen and cellulose, both of which form strong tension-bearing fibers with much larger diameters than microtubules. In the case of collagen, the primary structural element is tropocollagen, a triple helix (of linear polymers) which is about 300 nm long, 1.5 nm in diameter with a mass per unit length of about 1000 Da/nm. In turn, threads of tropocollagen form collagen fibrils, and these fibrils assemble in parallel to form collagen fibers.

The design of cellular filaments has been presented in some detail in order to illustrate both their similarities and differences. Most of the filaments possess a hierarchical organization of threads wound into strings, which then may be wound into ropes. The filaments within a cell are, to an order of magnitude, about 10 nm across, which is less than 1% of the diameters of the cells themselves. As one might expect, the visual appearance of the cytoskeletal filaments on cellular length scales varies with their thickness. The thickest filaments, microtubules, are stiff on the length scale of a micron, such that isolated filaments are only gently curved. In contrast, intertwined strings of spectrin are relatively flexible: at ambient temperatures, a 200 nm filament of spectrin adopts such convoluted shapes that the distance between its end-points is only 75 nm on average (for spectrin filaments that are part of a network).

The biological rods and ropes of a cell may undergo a variety of deformations, depending upon the nature of the applied forces and the mechanical properties of the filament. Analogous to the tension and compression experienced by the rigging and masts of a sailing ship, some forces lie along the length of the filament, causing it to stretch, shorten or perhaps buckle. In other cases, the forces are transverse to the filament, causing it to bend or twist. Whatever the deformation mode, energy may be required to distort the filament from its "natural" shape, by which we mean its shape at zero temperature and zero stress. Consider, for example, a uniform straight rod of length L bent into an arc of a circle of

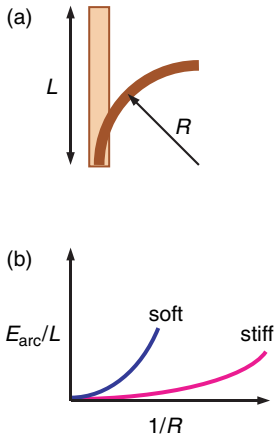

Fig. 3.2

Bending a rod of length L into the shape of an arc of radius R (in part (a)) requires an input of energy E_{arc} whose magnitude depends upon the severity of the deformation and the stiffness of the rod (b).

radius R, as illustrated in Fig. 3.2(a). Within a simple model introduced in Section 3.2 for the bending of rods, the energy E_{arc} required to perform this deformation is given by

$$E_{arc} = \kappa_f L / 2R^2, \tag{3.1}$$

where κ_f is called the flexural rigidity of the rod: large κ_f corresponds to stiff rods. Figure 3.2(b) displays how the bending energy behaves according to Eq. (3.1): a straight rod has $R = \infty$ (an infinite radius of curvature means that the rod is straight) and hence $E_{arc} = 0$, while a strongly curved rod might have L/R near unity, and hence $E_{arc} >> 0$, depending on the magnitude of κ_f.

The flexural rigidity of a uniform rod can be written as the product of its Young's modulus Y and the moment of inertia of its cross section $\mathcal{I}$,

$$\kappa_f = \mathcal{I} Y, \tag{3.2}$$

where Y and $\mathcal{I}$ reflect the composition and geometry of the rod, respectively. Stiff materials, such as steel, have $Y \sim 2 \times 10^{11}$ J/m^3, while softer materials, such as plastics, have $Y \sim 10^9$ J/m^3. The moment of inertia of the cross section, $\mathcal{I}$ (not to be confused with the moment of inertia of the mass, familiar from rotational motion), depends upon the shape of the rod; for instance, a cylindrical rod of constant density has $\mathcal{I} = \pi R^4/4$. Owing to its power-law dependence on filament radius, the flexural rigidity of filaments in the cell spans nearly five orders of magnitude.

We know from Chapters 1 and 2 that the energy of an object in thermal equilibrium fluctuates with time with an energy scale set by $k_B T$, such that an otherwise straight rod bends as it exchanges energy with its environment (see Fig. 3.3). The fluctuations in the local orientation of a sinuous filament can be characterized by the persistence length ξ_p that appears in the tangent correlation function introduced in Section 2.5: the larger the persistence length, the straighter a section of a rod will appear at a fixed

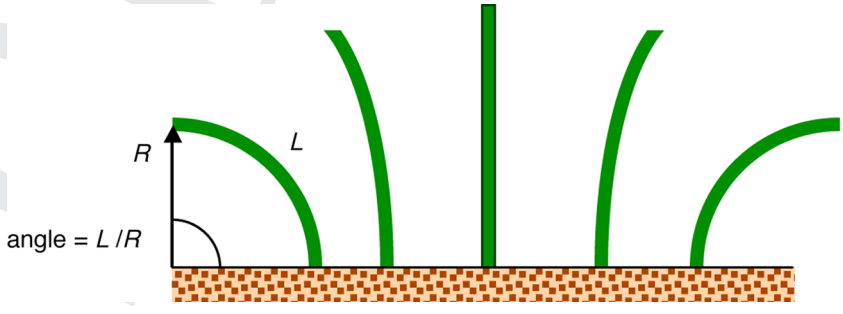

Fig. 3.3

Sample configurations of a very flexible rod at non-zero temperature as it exchanges energy with its surroundings. The base of the filament in the diagram is fixed. The configuration at the far left is an arc of a circle subtending an angle of L/R radians.

viewing distance. Intuitively, we expect that ξ_p should be directly proportional to the flexural rigidity κ_f (stiffer filaments are straighter) and inversely proportional to temperature $k_B T$ (colder filaments are straighter). A mechanical analysis shows that the combination $\kappa_f / k_B T$ is in fact the persistence length ξ_p of the filament

$$\xi_p = \kappa_f / k_B T = Y\mathcal{I} / k_B T, \tag{3.3}$$

as established in the treatment of shape fluctuations in Section 3.3.

If its persistence length is large compared to its contour length, i.e. $\xi_p >> L$, a filament appears relatively straight and recognizable as a rod. However, if $\xi_p << L$, the filament adopts more convoluted shapes, such as that in Fig. 3.4(a). What is the likelihood that a particular filament will be observed in one of its contorted shapes, as opposed to a rod-like one? Using the end-to-end displacement r_{ee} as a measure, there are many contorted shapes with r_{ee} close to zero, but very few extended ones with $r_{ee} \sim L$, as illustrated in Fig. 1.13 and Fig. 2.8. If there is little or no energy difference between these shapes compared to $k_B T$, then any specific configuration is as likely as any other and the filament will adopt a convoluted shape more frequently than a straight one. We can also view this conclusion in terms of entropy, which is proportional to the logarithm of the number of configurations available to a system (see Appendix C). The large family of shapes with $r_{ee}/L \approx 0$ contributes significantly to the system's entropy, while $r_{ee}/L \approx 1$ contributes much less.

Now consider what happens as we stretch a flexible filament by pulling on its ends, as in Fig. 3.4(b). Stretching the filament reduces the number of configurations available to it, thus lowering its entropy; thermodynamics tells us that this is not a desirable situation – systems do not spontaneously lower their entropy, all other things being equal. Because of this, a force must be applied to the ends of the filament to pull it straight and the filament is elastic by virtue of its entropy, as explained in Section 1.3.

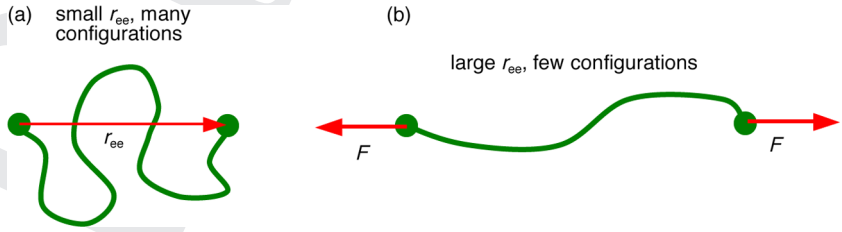

Fig. 3.4 Two samples from the set of configurations available to a highly flexible filament. The end-to-end displacement vector r_{ee} is indicated by the arrow in part (a). The number of configurations available at a given end-to-end distance is reduced as a force F is applied to the ends of the filament in (a) to stretch it out like that in (b).

For small extensions, this force is proportional to the change in r_{ee} from its equilibrium value, just like Hooke's Law for springs. In fact, the elastic behavior of convoluted filaments can be represented by an effective spring constant k_{sp} given by

$$k_{sp} = 3k_B T / 2L\xi_p, \tag{3.4}$$

which is valid for a filament in three dimensions near equilibrium (see Section 3.4).

We have emphasized the role of entropy in the structure and elastic properties of the cell's mechanical components simply because soft materials are so common. However, deformations of the relatively stiff components of the cell are dominated by energetic considerations familiar from continuum mechanics. Under a tensile force F, rods of length L, cross-sectional area A and uniform composition, stretch according to Hooke's Law $F = k_{sp}\,\Delta L$, where the spring constant k_{sp} is given by $k_{sp} = YA / L$. Under a compressive force, a rod first compresses according to Hooke's Law, but then buckles once a particular threshold F_{buckle} has been reached: $F_{buckle} = \pi^2 \kappa_f / L^2$. Microtubules may exhibit buckling during the cell division process of eukaryotic cells.

Thus, we see that filaments exhibit elastic behavior with differing microscopic origins. At low temperatures, a filament may resist stretching and bending for purely energetic reasons associated with displacing atoms from their most energetically favored positions. On the other hand, at high temperatures, the shape of a very flexible filament may fluctuate strongly, and entropy discourages such filaments from straightening out. In Sections 3.3 and 3.4, we investigate these situations using the formalism of statistical mechanics, but not until the bending of rods is expressed mathematically in Section 3.2. The buckling of rods under a compressive load is studied in Section 3.5, following which our formal results are applied to the analysis of biological polymers in Section 3.6. More details on the structure of filaments in the cytoskeleton can be found in Chapters 7–9 of Howard (2001).

3.2 Mathematical description of flexible rods

The various polymers and filaments in the cell display bending resistances whose numerical values span six orders of magnitude, from highly flexible alkanes through somewhat stiffer protein polymers such as F-actin, to moderately rigid microtubules. Viewed on micron length scales, these filaments may appear to be erratic, rambunctious chains or gently curved rods, and their elastic properties may be dominated by entropic or energetic

effects. In selecting a framework for interpreting the characteristics of cellular filaments, one can choose among several simple pictures of linear polymers, each picture emphasizing different aspects of the polymer. In this section, we view the filament as a smoothly curving rod in contrast to the wiggly segmented chain represented by a random walk (introduced in Section 2.3). These two pictures of linear polymers overlap, of course, and there are links between their parametrizations.

3.2.1 Arc length and curvature

Our primary interest at cellular length scales are filaments whose local orientation changes smoothly along their length. For the moment, the cross-sectional shape and material composition of the filament will be ignored so that it can be described as a continuous curve with no kinks or discontinuities. As displayed in Fig. 3.5(a), each point on the curve corresponds to a position vector $\mathbf{r}$, represented by the familiar Cartesian triplet (x, y, z). In Newtonian mechanics, we're already familiar with the idea of describing the trajectory of a projectile by writing its coordinates as a function of time, $\mathbf{r}(t)$, where t appears as a parameter. For the curve that represents a filament, we do something similar except $\mathbf{r}$ is written as a function of the arc length s [$\mathbf{r}(s)$ or the triplet $x(s)$, $y(s)$, $z(s)$], where s follows along the contour of the curve, running from 0 at one end to the full contour length L_c at the other. To illustrate how this works, consider a circle of radius R lying in the xy plane; the x and y coordinates of the circle are related to each other through the familiar equation $x^2 + y^2 = R^2$. In a parametric approach where the arc length s is used as a parameter, the coordinates are written as $x(s) = R\cos(s/R)$ and $y(s) = R\sin(s/R)$, where s is zero at $(x,y) = (R,0)$ and increases in a counter-clockwise fashion along the perimeter of the circle.

The function $\mathbf{r}(s)$ contains all the information needed to describe a sinuous curve, so that $\mathbf{r}(s)$ can be used to generate other characteristics of the

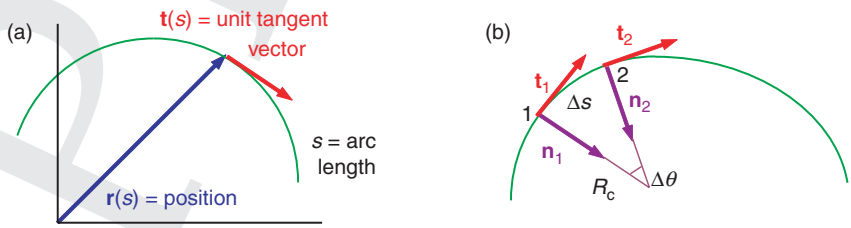

Fig. 3.5 (a) A point on the curve at arc length s is described by a position vector $\mathbf{r}(s)$ and a unit tangent vector $\mathbf{t}(s) = \partial\mathbf{r}/\partial s$. (b) Two locations are separated by an arc length Δs subtending an angle $\Delta\theta$ at a vertex formed by extensions of the unit normals $\mathbf{n}_1$ and $\mathbf{n}_2$. Extensions of $\mathbf{n}_1$ and $\mathbf{n}_2$ intersect at a distance R_c from the curve.

curve such as its local orientation. One of these is the unit tangent vector **t** that follows the direction of the curve as it winds its way through space, as shown in Fig. 3.5. In two dimensions, the (x,y) components of **t** are $(\cos\theta, \sin\theta)$, where θ is the angle between **t** and the x-axis. For a short section of arc Δs, over which the curve appears straight, the pair $(\cos\theta, \sin\theta)$ can be replaced by $(\Delta r_x/\Delta s, \Delta r_y/\Delta s)$, which becomes $(\partial r_x/\partial s, \partial r_y/\partial s)$ in the infinitesimal limit, or

$$\mathbf{t}(s) = \partial \mathbf{r}/\partial s. \tag{3.5}$$

Although Eq. (3.5) was derived as a two-dimensional example, it is valid in three dimensions as well.

How sinuous a curve appears depends on how rapidly **t** changes with s. Consider two nearby positions on a curve, which are labeled 1 and 2 on the curve illustrated in Fig. 3.5(b). If the curve were a straight line, the unit tangent vectors $\mathbf{t}_1$ and $\mathbf{t}_2$ at points 1 and 2 would be parallel; in other words, the orientations of the unit tangent vectors to a straight line are independent of position. However, such is not the case with curved lines. As we recall from introductory mechanics, the vector $\Delta\mathbf{t} = \mathbf{t}_2 - \mathbf{t}_1$ is perpendicular to the curve in the limit where positions 1 and 2 are infinitesimally close. Thus, the rate of change of **t** with s is proportional to the unit normal vector to the curve **n**, and we define the proportionality constant to be the curvature C

$$\partial \mathbf{t}/\partial s = C\mathbf{n}, \tag{3.6}$$

where C has units of inverse length. We can substitute Eq. (3.5) into (3.6) to obtain

$$C\mathbf{n} = \partial^2 \mathbf{r}/\partial s^2. \tag{3.7}$$

Some care must be taken about the direction of **n**. For example, consider the arc drawn in Fig. 3.5(b). Proceeding along the arc, one can see that $\Delta\mathbf{t}$ from location to location points to the "inside" or concave side of the arc, not the convex side.

The reciprocal of C is the local radius of curvature of the arc, as can be proven by extrapolating nearby unit normal vectors $\mathbf{n}_1$ and $\mathbf{n}_2$ to their point of intersection. In Fig. 3.5(b), positions 1 and 2 are close by on the contour and they define a segment that is approximately an arc of a circle with radius R_c. The segment has length Δs along the contour and subtends an angle $\Delta\theta = \Delta s / R_c$ with respect to the location where $\mathbf{n}_1$ and $\mathbf{n}_2$ intersect. However, $\Delta\theta$ is also the angle between $\mathbf{t}_1$ and $\mathbf{t}_2$; that is, $\Delta\theta = |\Delta\mathbf{t}| / t = |\Delta\mathbf{t}|$, the second equality following from $|\mathbf{t}| = t = 1$. Equating these two expressions for $\Delta\theta$ yields $|\Delta\mathbf{t}| / \Delta s = 1/R_c$, which can be compared with Eq. (3.6) to give

$$C = 1/R_c. \tag{3.8}$$

Lastly, the unit normal vector **n**, which is $\Delta\mathbf{t}/|\Delta\mathbf{t}|$, can itself be rewritten using $|\Delta\mathbf{t}| = \Delta\theta$

$$\mathbf{n} = \partial\mathbf{t}/\partial\theta, \tag{3.9}$$

in the limit where $\Delta\theta \to 0$.

3.2.2 Bending energy of a thin rod

The quantities $\mathbf{t}(s)$, $\mathbf{n}(s)$ and the local curvature C describe the shape of a flexible rod or rope, but they do not tell us the filament's dynamics. To understand the latter, we must find the forces or energies involved in deforming a filament by bending or twisting it. Suppose that we take a straight rod of length L_c with uniform density and cross section, and bend it into an arc with radius of curvature R_c, as in Fig. 3.3. The energy E_{arc} associated with this deformation is determined in many texts on continuum mechanics, and has the form (Landau and Lifshitz, 1986)

$$E_{arc}/L_c = \kappa_f / 2R_c^2 = Y\mathcal{I} / 2R_c^2. \tag{3.10}$$

Recalling Eq. (3.2), the flexural rigidity κ_f is equal to the product $Y\mathcal{I}$, where Y is Young's modulus of the material, and $\mathcal{I}$ is the moment of inertia of the cross section (see Fig. 3.6). Young's modulus appears in expressions of the form [*stress*] = Y [*strain*], and has the same units as stress, since strain is dimensionless (see Appendix D for a review of elasticity theory). For three-dimensional materials, Y has units of energy density, and typically ranges from 10^9 J/m^3 for plastics to 10^{11} J/m^3 for metals.

The moment of inertia of the cross section $\mathcal{I}$ is defined somewhat similarly to the moment of inertia of the mass: it is an area-weighted integral of the squared distance from an axis

$$\mathcal{I}_y = \int x^2 \, dA, \tag{3.11}$$

where the xy plane defined by the integration axes is a cross section perpendicular to the length of the rod, and dA is an element of surface area in that plane. The subscript y on the moment $\mathcal{I}$ indicates that the bending deformation occurs around the y-axis. It is generally advantageous to perform the integration in strips parallel to the y-axis so that the strips have constant values of x. For example, if the rod is a cylinder of radius R, the cross section has the shape of a solid disk with an area element dA at position x given by $dA = 2(R^2 - x^2)^{1/2}dx$, as shown in Fig. 3.6. Hence, for a solid cylinder

$$\mathcal{I}_y = 4\int_0^R x^2 \left(R^2 - x^2\right)^{1/2} dx = \pi R^4 / 4. \qquad \text{solid cylinder} \tag{3.12}$$

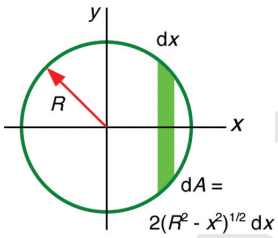

Fig. 3.6

Section through a cylindrical rod showing the *xy* axes used to evaluate the moment of inertia of the cross section $\mathcal{I}_y$ in Eq. (3.11).

Should the rod have a hollow core of radius R_i, like a microtubule, then the moment of inertia $\pi R^4/4$ of a solid cylinder would be reduced by the moment of inertia $\pi R_i^4/4$ of the core:

$$\mathcal{I}_y = \pi(R^4 - R_i^4)/4. \qquad \text{hollow cylinder} \tag{3.13}$$

Other rods of varying cross-sectional shape are treated in the end-of-chapter problems.

The deformation energy per unit length of the arc in Eq. (3.10) is inversely proportional to the square of the radius of curvature, or, equivalently, is proportional to the square of the curvature C from Eq. (3.8). In fact, one would expect on general grounds that the leading order contribution to the energy per unit length must be C^2, just as the potential energy of an ideal spring is proportional to the square of the displacement from equilibrium. Alternatively, then, the energy per unit length could be written as $E_{arc}/L = \kappa_f (\partial \mathbf{t}/\partial s)^2/2$ by using Eq. (3.6), an expression that is slightly closer mathematically to the functions representing the shape of the curve. For example, a straight line obeys $\partial \mathbf{t}/\partial s = 0$, for which the bending energy obviously vanishes. Further, there is no need for the curvature to be constant along the length of the filament, and the general expression for the total energy of deformation E_{bend} is, to lowest order,

$$E_{bend} = (\kappa_f / 2)\int_0^{L_c} (\partial \mathbf{t} / \partial s)^2 \, ds, \tag{3.14}$$

where the integral runs along the length of the filament. This form for E_{bend} is called the Kratky–Porod model; it can be trivially modified to represent a rod that is intrinsically curved even when it is not under stress.

3.2.3 Directional fluctuations and persistence length

At zero temperature, a filament adopts a shape that minimizes its energy, which corresponds to a straight rod if the energy is governed by Eq. (3.14). At non-zero temperature, the filament exchanges energy with its environment, permitting the shape to fluctuate, as illustrated in Fig. 3.7(a). According to Eq. (3.14), the bending energy of a filament rises as its shape becomes more contorted and the local curvature along the filament grows; hence, the bending energy of the configurations increases from left to right in Fig. 3.7(a). Now, the probability $\mathcal{P}(E)$ of the filament being found in a specific configuration with energy E is proportional to the Boltzmann factor $\exp(-\beta E)$, where β is the inverse temperature $\beta = 1/k_B T$ (see Appendix C for a review). The Boltzmann factor tells us that the larger the energy required to deform the filament into a specific shape, the lower the probability that the filament will have that shape, all other things being equal. Thus, a filament will adopt configurations with small average curvature if its flexural rigidity is high or the temperature is low; the shapes will resemble sections of circles, becoming contorted only at high temperatures.

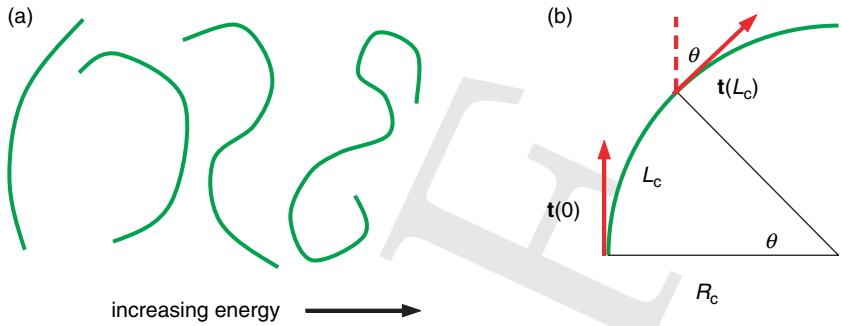

Fig. 3.7 (a) Sample of configurations available to a filament; for a given κ_f the bending energy of the filament rises as its shape becomes more contorted. (b) If the filament is a section of a circle, the angle subtended by the contour length L_c is the same as the change in the direction of the unit tangent vector **t** along the arc.

Let's now examine the bending energy of a specific filament that can sustain only gentle curves; its contour length is sufficiently short that the curvature of the bend is constant. The shape can then be uniquely parametrized by the angle θ between the unit tangent vectors $\mathbf{t}(0)$ and $\mathbf{t}(L_c)$ at the two ends of the filament as in Fig. 3.7(b). This angle is the same as that subtended by the contour length (i.e. $\theta = L_c/R_c$) because we have taken the shape to be an arc of a circle with a radius R_c. Thus, each configuration has a bending energy determined by the value of θ

$$E_{arc} = \kappa_f \theta^2 / 2L_c, \tag{3.15}$$

where we have removed R_c from Eq. (3.10) in favor of θ by using $R_c = L_c/\theta$.

At non-zero temperature, the angle θ changes as the filament waves back and forth exchanging energy with its thermal environment: at higher temperatures, the oscillations have a larger amplitude and the filament samples larger values of θ than at lower temperatures. To characterize the magnitude of the oscillations, we evaluate the mean value of θ^2, denoted by the conventional $\langle \theta^2 \rangle$. If the filament has a fixed length, $\langle \theta^2 \rangle$ involves a weighted average of the three-dimensional position sampled by the end of the filament. That is, with one end of the filament defining the direction of a coordinate axis (say the z-axis), the other end is described by the polar angle θ and the azimuthal angle ϕ, such that the ensemble average is

$$\langle \theta^2 \rangle = \int \theta^2 \mathcal{P}(E_{arc}) d\Omega / \int \mathcal{P}(E_{arc}) d\Omega, \tag{3.16}$$

where E_{arc} is given by Eq. (3.15) and where the integral must be performed over the solid angle $d\Omega = \sin\theta \, d\theta \, d\phi$. The bending energy E_{arc} is independent of ϕ, allowing the azimuthal angle to be integrated out, leaving

$$\langle \theta^2 \rangle = \int \theta^2 \, \mathcal{P}(E_{\text{arc}}) \sin\theta \, d\theta \, / \int \mathcal{P}(E_{\text{arc}}) \sin\theta \, d\theta, \tag{3.17}$$

where the range of θ in the integrals is 0 to 2π.

In thermal equilibrium, the probability $\mathcal{P}(E_{\text{arc}})$ of finding a configuration with a given bending energy E_{arc} is given by the Boltzmann factor $\exp(-\beta E_{\text{arc}})$, so that Eq. (3.17) becomes

$$\langle \theta^2 \rangle = \int \theta^2 \exp(-\beta E_{\text{arc}}) \sin\theta \, d\theta \, / \int \exp(-\beta E_{\text{arc}}) \sin\theta \, d\theta. \tag{3.18}$$

According to Eq. (3.15), the bending energy E_{arc} rises quadratically with θ, with the result that the Boltzmann factor decays rapidly with θ. Conseqently, the $\sin\theta$ factors in Eq. (3.18) are sampled only at small θ, and can be replaced by the small angle approximation $\sin\theta \sim \theta$. Hence, Eq. (3.18) becomes

$$\langle \theta^2 \rangle = (2L_c / \beta\kappa_f) \int x^3 \exp(-x^2) \, dx \, / \int x \exp(-x^2) \, dx, \tag{3.19}$$

after substituting Eq. (3.15) for E_{arc} and changing variables to $x = (\beta\kappa_f / 2L_c)^{1/2}\theta$. In the small oscillation approximation, the upper limits of the integrals in Eq. (3.19) can be extended to infinity with little error, whence both integrals are equal to 1/2 and cancel out. Thus, the expression for the mean square value of θ is

$$\langle \theta^2 \rangle \cong 2s / \beta\kappa_f, \qquad \text{small oscillations} \tag{3.20}$$

where we have replaced L_c by the arc length s in anticipation of making the contour length a variable. The combination $\beta\kappa_f$ has the units of length, and is defined as the persistence length ξ_p of the filament:

$$\xi_p \equiv \beta\kappa_f. \tag{3.21}$$

Note that, for thermal systems, ξ_p decreases with increasing temperature.

A directional persistence length ξ was introduced in Section 2.5 by means of the tangent correlation function $\langle \mathbf{t}(0) \cdot \mathbf{t}(s) \rangle$, and we will now show that ξ and ξ_p are one and the same. Still assuming that the shapes of the filament are arcs of circles, the ensemble average $\langle \mathbf{t}(0) \cdot \mathbf{t}(s) \rangle = \langle \cos\theta \rangle$, which has a maximum absolute value of unity because $|\mathbf{t}| = 1$. At low temperatures where θ is usually small, we again invoke the small approximation that leads from Eq. (3.18) to Eq. (3.19): $\cos\theta \sim 1 - \theta^2/2$, permitting the correlation function to be written as

$$\langle \mathbf{t}(0) \cdot \mathbf{t}(s) \rangle \sim 1 - \langle \theta^2 \rangle / 2. \tag{3.22}$$

The variance in θ in this small oscillation limit is given by Eq. (3.20), so that

$$\langle \mathbf{t}(0) \cdot \mathbf{t}(s) \rangle \sim 1 - s/\xi_p \qquad (s/\xi_p << 1), \tag{3.23}$$

where the arc length s now appears as a parameter: the equation is valid for filaments of varying length. Equation (3.23) can be used to obtain the mean squared difference in the tangent vectors

$$\langle [\mathbf{t}(s) - \mathbf{t}(0)]^2 \rangle = 2 - 2\langle \mathbf{t}(0) \cdot \mathbf{t}(s) \rangle \sim 2s/\xi_p \qquad (s/\xi_p << 1). \tag{3.24}$$

When a filament's contour length is short compared with ξ_p, Eq. (3.23) correctly predicts that $\langle \mathbf{t}(0) \cdot \mathbf{t}(L_c) \rangle$ initially dies off linearly as L_c grows. However, if $L_c >> \xi_p$, the filament appears floppy and $\langle \mathbf{t}(0) \cdot \mathbf{t}(L_c) \rangle$ should vanish as the tangent vectors at the ends of the filament become uncorrelated, a regime not included in Eq. (3.23) because it was derived in the limit of small oscillations. Rather, the correct expression for the tangent correlation function applicable at short and long distances is

$$\langle \mathbf{t}(0) \cdot \mathbf{t}(s) \rangle = \exp(-s/\xi_p), \tag{3.25}$$

from which we see that Eq. (3.23) is the leading order approximation via $\exp(-x) \sim 1 - x$ at small x. Intuitively, one would expect to obtain an expression like Eq. (3.25) by applying Eq. (3.23) repeatedly to successive sections of the filament; a more detailed derivation can be found in Doi and Edwards (1986).

3.3 Sizes of polymer chains

A function of both temperature and bending resistance, the persistence length of a filament sets the length scale of its thermal undulations. If the contour length of the filament is much smaller than its persistence length, the filament can be viewed as a relatively stiff rod undergoing only limited excursions from its equilibrium shape. In contrast, a very flexible polymer samples an extensive collection of contorted shapes with erratically changing directions. Do the configurations in this collection have any large scale characteristics, or are they just an unruly mob of rapidly changing tangents and curvatures? If the ensemble of configurations do have common or universal features, upon what properties of the filament do they depend? Here, we study several polymer families, characterized by their connectivity and interactions, to answer these questions.

3.3.1 Ideal chains and filaments

In Section 2.3, we derive several properties of ideal random walks, and establish that the mean square value of the end-to-end displacement vector $\mathbf{r}_{ee}$ obeys $\langle r_{ee}^2 \rangle = Nb^2$, where N is the number of steps in the walk and b is the length of each step (assumed identical for all steps). We argue that flexible polymers might be described by such walks, and apply the expression for $\langle r_{ee}^2 \rangle$ to floppy proteins to demonstrate how the radius of its folded state should be much less than its contour length. We now perform the same kind of analysis to the continuous representation of flexible

filaments introduced in Section 3.2, rather than the segmented configurations of Section 2.3.

We start with the conventional end-to-end displacement vector $\mathbf{r}_{ee} \equiv \mathbf{r}(L_c) - \mathbf{r}(0)$, where $\mathbf{r}(s)$ is the continuous function that denotes the position of the filament at arc length s. The mean square value of $\mathbf{r}_{ee}$ is then

$$\langle \mathbf{r}_{ee}{}^2 \rangle = \langle [\mathbf{r}(L_c) - \mathbf{r}(0)]^2 \rangle. \tag{3.26}$$

The unit tangent vector $\mathbf{t}(s)$ was introduced in Eq. (3.5) as a derivative of the position $\mathbf{r}(s)$, which means that $\mathbf{r}(s)$ at any location can be found by integrating $\mathbf{t}(s)$, as in

$$\mathbf{r}(s) = \mathbf{r}(0) + \int_0^s \mathrm{d}u\ \mathbf{t}(u). \tag{3.27}$$

The representation of $\mathbf{r}(s)$ in Eq. (3.27) can be substituted into Eq. (3.26) to yield

$$\langle \mathbf{r}_{ee}{}^2 \rangle = \int_0^{L_c} \mathrm{d}u \int_0^{L_c} \mathrm{d}v \langle \mathbf{t}(u) \bullet \mathbf{t}(v) \rangle, \tag{3.28}$$

after moving the ensemble average inside the integral. According to Eq. (3.25), the correlation function $\langle \mathbf{t}(s) \bullet \mathbf{t}(0) \rangle$ decays exponentially as $\exp(-s/\xi_p)$, which means that Eq. (3.28) can be rewritten as

$$\langle \mathbf{r}_{ee}{}^2 \rangle = \int_0^{L_c} \mathrm{d}u \int_0^{L_c} \mathrm{d}v\ \exp\left(-|u-v|/\xi_p\right). \tag{3.29}$$

The absolute value operation in the exponential looks slightly awkward, but it can be handled by breaking the integral into two identical pieces where one integration variable is forced to have a value less than the other during integration:

$$\langle \mathbf{r}_{ee}{}^2 \rangle = 2 \int_0^{L_c} \mathrm{d}u \int_0^{u} \mathrm{d}v\ \exp\left(-[u-v]/\xi_p\right). \tag{3.30}$$

It is straightforward to solve this integral using a few changes of variables

$$\begin{aligned} 2 \int_0^{L_c} \exp\left(-u/\xi_p\right)\ \mathrm{d}u \int_0^{u} \mathrm{d}v\ \exp\left(v/\xi_p\right) & \\ = 2 \int_0^{L_c} \mathrm{d}u\ \exp\left(-u/\xi_p\right) \bullet\ \xi_p \bullet \left[\exp\left(u/\xi_p\right) - 1\right] & \\ = 2\xi_p{}^2 \int_0^{L_c/\xi_p} \mathrm{d}w\ \left[1 - \exp(-w)\right]. & \end{aligned} \tag{3.31}$$

Evaluating the last integral gives

$$\langle \mathbf{r}_{ee}{}^2 \rangle = 2\xi_p L_c - 2\xi_p{}^2 [1 - \exp(-L_c/\xi_p)]. \qquad \text{continuous curve} \qquad (3.32)$$

This result simplifies in two limits. If $\xi_p >> L_c$, Eq. (3.32) reduces to $\langle \mathbf{r}_{ee}{}^2 \rangle^{1/2} = L_c$ using the approximation $\exp(-x) \sim 1 - x + x^2/2\ldots$ valid at small x; in this limit, the filament appears rather rod-like with an end-to-end displacement close to its contour length. At the other extreme where $\xi_p << L_c$, Eq. (3.32) is approximately

$$\langle \mathbf{r}_{ee}{}^2 \rangle \cong 2\xi_p L_c \quad (\text{if } L_c >> \xi_p), \qquad (3.33)$$

implying that, over long distances compared to the persistence length, $\langle \mathbf{r}_{ee}{}^2 \rangle^{1/2}$ grows like the square root of the contour length, not as the contour length itself. In other words, long polymers appear convoluted, and their average linear dimension increases much more slowly than their contour length.

The behavior of $\langle \mathbf{r}_{ee}{}^2 \rangle$ for continuous filaments with $\xi_p << L_c$ is the same as that of ideal segmented chains $\langle r_{ee}{}^2 \rangle = Nb^2$ once Nb is replaced by the contour length L_c and the step size is identified with $2\xi_p$ in Eq. (3.33) such that

$$\xi_p = b/2. \qquad \text{ideal chains} \qquad (3.34)$$

In other words, both descriptions show that the linear dimension of very flexible filaments increases as the square root of the contour length. The scaling behavior $\langle \mathbf{r}_{ee}{}^2 \rangle^{1/2} \sim N^{1/2}$ or $L_c{}^{1/2}$ in Eqs. (2.31) and (3.33) is referred to as *ideal* scaling. Note that our determination of the ideal scaling exponent does not depend on the dimension of the space in which the chain resides: random chains in two dimensions (i.e. confined to a plane) or three dimensions both exhibit the same scaling behavior.

Ideal scaling of polymer chains can appear even if the orientations of neighboring segments are not completely random, although the persistence length of the polymer will not be $b/2$. As an example, consider the usual set of bond vectors $\{\mathbf{b}_i\}$ from which the end-to-end displacement vector is constructed via $\mathbf{r}_{ee} = \Sigma_{i=1,N} \mathbf{b}_i$. In the freely rotating chain model, successive chain elements $\mathbf{b}_i$ and $\mathbf{b}_{i+1}$ are forced to have the same polar angle α, although the bonds may swivel around each other and each bond has the same length b. As usual, the ensemble average $\langle \mathbf{r}_{ee}{}^2 \rangle$ has the formal representation

$$\langle \mathbf{r}_{ee}{}^2 \rangle = \Sigma_i \Sigma_j \langle \mathbf{b}_i \bullet \mathbf{b}_j \rangle,$$

but there are now restrictions present within $\langle \cdots \rangle$. This model is solved in the end-of-chapter problems (see also Flory (1953), p. 414), and yields

$$\langle \mathbf{r}_{ee}{}^2 \rangle = Nb^2 (1 - \cos\alpha) / (1 + \cos\alpha), \qquad (3.35)$$

in the large N limit.

Now, $\langle \mathbf{r}_{ee}{}^2 \rangle^{1/2}$ in Eq. (3.35) obeys the scaling exponent $N^{1/2}$, demonstrating that self-intersecting freely rotating chains are ideal. Further, Eq. (3.35)

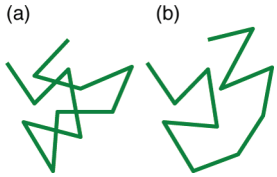

Fig. 3.8

Self-avoidance changes the scaling properties of chains in one-, two- and three-dimensional systems. In the two-dimensional configurations displayed here, (a) is a random chain and (b) is a self-avoiding chain.

reduces to the form Nb^2 if the length scale is changed to $b\,[(1-\cos\alpha)/(1+\cos\alpha)]^{1/2}$, suggesting that an *effective bond length* B_{eff} can be defined for freely rotating chains via

$$B_{\text{eff}} = b\,[(1-\cos\alpha)/(1+\cos\alpha)]^{1/2}, \tag{3.36}$$

and $\langle \mathbf{r}_{\text{ee}}^2 \rangle$ is expressed as NB_{eff}^2. The effective bond length is only one of the parametrizations commonly employed for ideal chains with N segments:

$$\langle \mathbf{r}_{\text{ee}}^2 \rangle = \begin{cases} NB_{\text{eff}}^2 \\ L_c \mathcal{L}_K \\ 2L_c \xi_p. \end{cases} \tag{3.37}$$

Another parametrization is the Kuhn length, $\mathcal{L}_K$, defined in analogy with the monomer length: $\langle \mathbf{r}_{\text{ee}}^2 \rangle = N_K \mathcal{L}_K^2$ and $L_c = N_K \mathcal{L}_K$, with N_K the number of Kuhn lengths in the contour length.

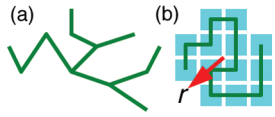

Fig. 3.9

Sample configurations of a branched polymer (a) and a dense chain (b) in two dimensions. To aid the argument in the text, the chain in (b) consists of linked squares, which, when packed tightly together, cover an area $\sim r^2$ in two dimensions.

3.3.2 Self-avoiding linear chains

Our treatment of random chains places no restriction on the interaction between chain segments: nothing in the mathematical representation of the chains prevents the displacement vectors from crossing one another. However, physical systems have an excluded volume that enforces self-avoidance of the chain, as illustrated in Fig. 3.8 for two-dimensional chains. This steric interaction among the chain elements is important for chains in one-, two- and three-dimensional systems. As an illustration, consider the simple situation in which a chain lies along the x-axis. Self-avoidance forbids the chain from reversing on itself from one step to the next, so that the end-to-end distance must be just the contour length Nb: i.e. $\langle \mathbf{r}_{\text{ee}}^2 \rangle^{1/2} \sim N^1$ for a straight chain in one dimension. But Eq. (2.31) shows that $\langle \mathbf{r}_{\text{ee}}^2 \rangle^{1/2}$ for ideal chains scales like $N^{1/2}$, *independent of embedding dimension*. Thus, we conclude that in one dimension, self-avoidance of a chain dramatically affects its scaling properties: N^1 for self-avoiding chains and $N^{1/2}$ for ideal chains. Similar conclusions can be drawn for chains in two and three dimensions, although the scaling exponents are different. As shown by Flory, rather general arguments lead to the prediction that the scaling exponents of self-avoiding linear chains should obey (see Section 8.4)

$$\nu_{\text{FL}} = 3/(2+d), \tag{3.38}$$

where d is the embedding dimension. Equation (3.38) gives $\nu_{\text{FL}} = 1$, 3/4, 3/5 and 1/2, in one to four dimensions, respectively, predictions which have been shown to be exact or nearly so. As the ideal scaling exponent cannot be less than 1/2, Eq. (3.38) is not valid in more than four dimensions; hence, the effects of self-avoidance are irrelevant in four or more dimensions and the scaling is always ideal.

3.3.3 Branched polymers

The polymers discussed in most of this text are linear chains; however, there are many examples of polymers with extensive side branches. The scaling behavior of such *branched polymers* should not be the same as single chains, since branching adds more monomers along the chain length as illustrated in Fig. 3.9(a). Because a branched polymer has more than two ends, the end-to-end displacement has to be replaced by a different measure of the polymer size, such as the radius of gyration, R_g (see end-of-chapter problems). The radius of gyration for branched polymers is found to have a scaling form

$$\langle R_g^2 \rangle^{1/2} \sim N^{\nu}, \tag{3.39}$$

where N is the number of polymer segments and $\nu = 0.64$ and 0.5 in two and three dimensions, respectively (see Section 8.4). In comparison, self-avoiding linear chains have scaling exponents of 3/4 and 0.59, respectively (see Eq. (3.38)), meaning that the spatial region occupied by branched polymers grows more slowly with N than does that of linear chains; i.e. linear chains are less dense than branched polymers. Fluid membranes also behave like branched polymers at large length scales (see Section 8.4).

3.3.4 Collapsed chains

None of the chain configurations described so far in this section is as compact as it could be. Consider a system of identical objects, say squares in two dimensions or cubes in three dimensions, having a length b to the side such that each object has a "volume" of b^d in d dimensions, and N of these objects have a volume Nb^d. The configuration of the N objects with the smallest surface area is the most compact or the most *dense* configuration, as illustrated in Fig. 3.9(b), and we denote by r the linear dimension of this configuration. Ignoring factors of π and the like, the total volume Nb^d of the most compact configuration is proportional to r^d, so that r itself scales like

$$r \sim N^{1/d} \text{ (dense)}. \tag{3.40}$$

Polymers can be made to collapse into their most dense configurations by a variety of experimental means, including changes in the solvent, and it is observed that the collapse of the chains occurs at a well-defined phase transition.

The scaling exponents of all the systems that we have considered in this section are summarized in Table 3.1. If the chains are self-avoiding, $1/d$ represents the lower bound on the possible values of the scaling exponents for the "size" of the configurations, and the straight rod scaling of $\langle R_g^2 \rangle^{1/2} \sim N^1$ represents the upper bound. One can see from the table that random or

Table 3.1 Exponents for the scaling law $\langle R_g^2 \rangle^{1/2} \sim N^{\nu}$ for ideal (or random) chains, self-avoiding chains and branched polymers, as a function of embedding dimension d. Collapsed chains have the highest density and obey $\langle R_g^2 \rangle^{1/2} \sim N^{1/d}$.

Configuration	$d = 2$	$d = 3$	$d = 4$
Ideal chains	1/2	1/2	1/2
Self-avoiding chains	3/4	0.59	1/2
Branched polymers	0.64	1/2	
Collapsed chains	1/2	1/3	1/4

self-avoiding chains, as well as branched polymers, exhibit scaling behavior that lies between these extremes.

3.4 Entropic elasticity

The distribution of end-to-end displacements $\mathbf{r}_{ee}$ for random walks in one dimension was derived in Section 2.3; viewing the walks as one-dimensional linear polymers, it was argued that entropy favored polymer configurations that were convoluted rather than straight. In this section, the analysis is extended to walks or polymer chains in three dimensions, which allows for a larger variety of configurations. The three-dimensional distributions confirm that it is highly unlikely for a random chain to be found in a fully stretched configuration: the most likely value of r_{ee}^2 for a freely jointed chain is not far from its mean value of Nb^2, for chains with N links of length b. Consequently, as a polymer chain is made to straighten out by an external force, its entropy decreases and work must be done on the chain to stretch it: in other words, the polymer behaves elastically because of its entropy. Here, we will establish that the Hooke's law spring constant associated with a polymer's entropic resistance to stretching increases with temperature as $3k_BT / Nb^2$ for three-dimensional chains.

3.4.1 Random chain in three dimensions

Let us briefly revisit the results from Section 2.3 for ideal random walks: the mean squared end-to-end displacement obeys $\langle r_{ee}^2 \rangle = Nb^2$ in any dimension, while the probability distribution for $r_{ee,x}$ in one dimension obeys $\mathcal{P}(x) \propto \exp(-r_{ee,x}^2 / 2\sigma^2)$, where $\sigma^2 \equiv Nb^2$. How does the probability change in three dimensions? By projecting their configurations onto a set of Cartesian axes, as illustrated in Fig. 3.10, three-dimensional random

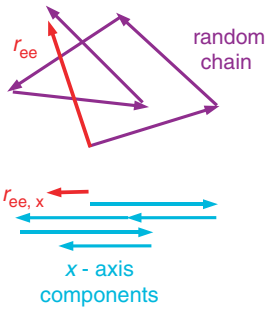

Fig. 3.10

Projection of the segments of a two-dimensional chain onto the x-axis.

chains can be treated as three separate one-dimensional systems. For example, the x-component of the end-to-end displacement vector, $r_{ee,x}$, is just the sum of the individual monomer vectors as projected onto the x-axis:

$$r_{ee,x} = \Sigma_i \, b_{i,x}, \tag{3.41}$$

where $b_{i,x}$ is the x-projection of the monomer vector $\mathbf{b}_i$. For freely jointed chains, the component $b_{i,x}$ is independent of the component $b_{i+1,x}$, so the projections form a random walk in one dimension, although the x-axis projections are of variable length even if all monomers have the same b in three dimensions. If the number of segments is large, the probability distribution with variable segment length has the same form as the distribution with uniform segment length (Chapter 1 of Reif, 1965),

$$\mathcal{P}(x) = (2\pi\sigma_x^2)^{-1/2} \exp(-r_{ee,x}^2 / 2\sigma_x^2), \tag{3.42}$$

except that the variance is given by

$$\sigma_x^2 = N\langle b_x^2 \rangle. \tag{3.43}$$

In this variance, b^2 of the strictly one-dimensional walk with fixed step size has been replaced by $\langle b_x^2 \rangle \le b^2$ for variable step size. Of course, one could still say that Eq. (3.43) incorporates the strictly one-dimensional case, in that $\langle b_x^2 \rangle = b^2$ if the step size is constant.

It is straightforward to determine $\langle b_x^2 \rangle$ even when the projected steps are of unequal length. The expectation of the step length in three dimensions must have the form

$$\langle b^2 \rangle = \langle b_x^2 + b_y^2 + b_z^2 \rangle = \langle b_x^2 \rangle + \langle b_y^2 \rangle + \langle b_z^2 \rangle. \tag{3.44}$$

Because of symmetry, we anticipate that the mean projections must be the same along each of the Cartesian axes, so

$$\langle b_x^2 \rangle = \langle b_y^2 \rangle = \langle b_z^2 \rangle = b^2/3. \tag{3.45}$$

Hence, the variance in Eq. (3.43) is

$$\sigma_3^2 \equiv \sigma_x^2 = Nb^2/3, \qquad \sigma_3^2 \text{ in three dimensions} \tag{3.46}$$

where we have introduced the new symbol σ_3 just to avoid notational confusion between one- and three-dimensional walks.

Equation (3.42) is the probability density for $\mathbf{r}_{ee}$ as projected onto the x-axis. By symmetry, similar expressions exist for the y- and z-axis projections. These three distributions can be combined to give the probability density for finding $\mathbf{r}_{ee}$ in a volume $dx\,dy\,dz$ centered on the specific position (x,y,z), namely $\mathcal{P}(x,y,z)\,dx\,dy\,dz$. Thus, $\mathcal{P}(x,y,z)$ is the product of the probability distributions in each of the Cartesian directions

$$\mathcal{P}(x,y,z) = \mathcal{P}(x)\,\mathcal{P}(y)\,\mathcal{P}(z) = (2\pi\sigma_3^2)^{-3/2} \exp[-(x^2+y^2+z^2) / 2\sigma_3^2], \tag{3.47}$$

where σ_3^2 is still given by Eq. (3.46), and where $x \equiv r_{ee,x}$, etc. Equation (3.47) says that, of all possible chain configurations, the most likely set of coordinates for the tip of the chain is (0,0,0), which is the coordinate origin of the chain or random walk; it does *not* say that the most likely value of r_{ee} is zero. Indeed, the distribution of the magnitude of $\mathbf{r}_{ee}$ must reflect the fact that many different coordinate positions (x,y,z) have the same r, although $\mathbf{r}_{ee}$ may point in various directions at that value of r. The probability for the chain to have a radial end-to-end distance between r and $r + dr$ is $\mathcal{P}_{rad}(r)\, dr$, where $\mathcal{P}_{rad}(r)$ is the probability per unit length obtained from

$$\int_{angle} \mathcal{P}(x,y,z)\, dx\, dy\, dz = \mathcal{P}_{rad}(r)\, dr. \tag{3.48}$$

Replacing $dx\, dy\, dz$ by the angular expression $r^2\, dr \sin\theta\, d\theta\, d\phi$, the θ and ϕ integrals in Eq. (3.48) can be done immediately, as $x^2+y^2+z^2 = r^2$ so that there is no angular dependence on the right-hand side of Eq. (3.47). Thus,

$$\mathcal{P}_{rad}(r) = 4\pi r^2\, (2\pi\sigma_3^2)^{-3/2} \exp(-r^2 / 2\sigma_3^2). \tag{3.49}$$

It's the extra factor of r^2 outside of the exponential that shifts the most likely value of r_{ee} away from zero.

Figure 3.11 shows the behavior of Eq. (3.49), as well as the projection of the chain on the x-axis. We can equate to zero the derivative of $\mathcal{P}_{rad}(r)$ with respect to r to find the most likely value of r_{ee}. A summary of the results for ideal chains in three dimensions is:

$$r_{ee,\,\text{most likely}} = (2/3)^{1/2}\, N^{1/2} b, \tag{3.50}$$

$$\langle r_{ee} \rangle = (8/3\pi)^{1/2}\, N^{1/2} b, \tag{3.51}$$

and, of course,

$$\langle \mathbf{r}_{ee}^2 \rangle = N b^2. \tag{3.52}$$

Note that r_{ee} in Eqs. (3.50) and (3.51) is the scalar radius $r_{ee} = (\mathbf{r}_{ee}^2)^{1/2}$.

3.4.2 Entropic elasticity

The probability distribution functions, as illustrated in Fig. 3.11, confirm our intuition that far more chain configurations have end-to-end displacements close to the mean value of r_{ee} than to the chain contour length L_c. Being proportional to the logarithm of the number of configurations, the entropy S of a polymer chain must decrease as the chain is stretched from its equilibrium length. Now the free energy of an ensemble of chains at a temperature T is $F = E - TS$, which is simply $F = -TS$ for freely jointed

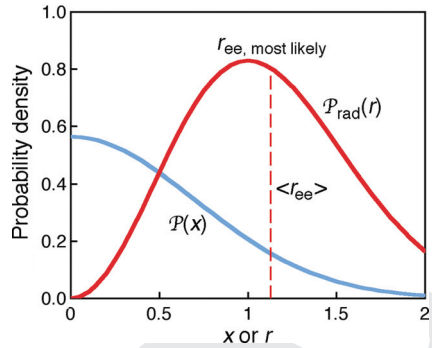

Fig. 3.11 Probability distributions for random chains in three dimensions. Two cases are shown: the three-dimensional distribution (red curve) as a function of $r = r_{ee}$, and the x-axis projection (blue curve) as a function of $x = r_{ee,x}$ ($\sigma^2 = 1/2$ in both distributions). The dashed vertical line is $\langle r_{ee} \rangle$ in three dimensions.

chains, since their configurations all have vanishing energy E. Thus, S decreases and F increases as the chain is stretched at non-zero temperature; in other words, work must be done to stretch the chain, and the chain is elastic by virtue of its entropy.

Viewed as a spring obeying Hooke's Law, the effective force constant of a polymer chain can be extracted by comparing the distributions for the end-to-end displacement of the chain with that of an ideal spring, whose fluctuations can be calculated using statistical mechanics. Now, a Hookean spring has a potential energy $V(x)$ equal to $k_{sp}x^2/2$, where x is the displacement from equilibrium and k_{sp} is the force constant of the spring. Aside from an overall normalization factor, the probability distribution $\mathcal{P}(x)$ for the spring displacement x is proportional to the usual Boltzmann factor $\exp(-E/k_BT)$, which becomes, for the Hooke's Law potential

$$\mathcal{P}(x) \sim \exp(-k_{sp}x^2 / 2k_BT). \tag{3.53}$$

The probability distribution for the displacement of an ideal chain according to Eq. (3.42) is $\mathcal{P}(x) \sim \exp(-x^2/2\sigma_d^2)$, again aside from an overall normalization factor. Comparing the functional form of the two distributions at large x gives $k_{sp} = k_BT/\sigma_d^2$, where $\sigma_d^2 = Nb^2/d$ for ideal chains embedded in d dimensions [the dimensionality can be seen from Eq. (3.46)]. Hence, in three dimensions, we expect

$$k_{sp} = 3k_BT / Nb^2 = 3k_BT / 2\xi_pL_c, \qquad k_{sp} \text{ in three dimensions} \tag{3.54}$$

using $L_c = Nb$ and $\xi_p = b/2$ for an ideal chain. Observe that k_{sp} increases with temperature, which is readily demonstrated experimentally by hanging a

weight from an elastic band, and then using a device (like a hair dryer) to heat the elastic. The weight will be seen to rise as the elastic heats up, since k_{sp} increases simultaneously and provides greater resistance to the stretching of the elastic band by the weight.

3.4.3 Highly stretched chains

The Gaussian probability distribution, Eq. (3.42), gives a good description of chain behavior at small displacements from equilibrium. It predicts, from Eq. (3.54), that the force f required to produce an extension x in the end-to-end displacement is $f = (3k_BT / 2\xi_pL_c)x$, which can be rewritten as

$$x/L_c = (2\xi_p / 3k_BT)\, f. \tag{3.55}$$

If the chain segments are individually inextensible, the force required to extend the chain should diverge as the chain approaches its maximal extension, $x/L_c \to 1$. Such a divergence is not present in Eq. (3.55), indicating that the Gaussian distribution must be increasingly inaccurate and ultimately invalid as an inextensible chain is stretched towards its contour length.

Of course, the Gaussian distribution is only an approximate representation of freely jointed chains; fortunately, the force–extension relation of rigid, freely jointed rods can be obtained analytically. For those familiar with the example, the problem is analogous to the alignment of spin vectors in an external field, where the spin vectors represent the projection of the polymer segments along the direction of the applied field. It is straightforward to show (Kuhn and Grün, 1942; James and Guth, 1943; see also Flory, 1953, p. 427) that the solution has the form

$$x/L_c = \mathcal{L}(2\xi_p f / k_BT), \tag{3.56}$$

where $\mathcal{L}(y)$ is the Langevin function

$$\mathcal{L}(y) = \coth(y) - 1/y. \tag{3.57}$$

Note that x in Eq. (3.56) is the projection of the end-to-end displacement along the direction of the applied force. For small values of f, Eq. (3.56) reduces to the Gaussian expression Eq. (3.55); for very large values of f, the Langevin function tends to 1 so that x asymptotically approaches L_c in Eq. (3.56), as desired.

The force–extension relation of freely jointed rods provides a reasonably accurate description of biopolymers. Its weakness lies in viewing the polymer as a chain of rigid segments: thick filaments such as microtubules and DNA surely look more like continuously flexible ropes than chains of rigid rods. A more appropriate representation of flexible filaments can be derived from the Kratky–Porod energy expression, Eq. (3.14), and is referred to as the worm-like chain (WLC). Although the

general form of the WLC force–extension relationship is numerical, an accurate interpolation formula has been obtained by Marko and Siggia (1995):

$$\xi_p f / k_B T = (1/4)(1 - x/L_c)^{-2} - 1/4 + x/L_c. \quad (3.58)$$

Again, the force diverges in this expression as $x/L_c \to 1$, as desired. Equation (3.58) and the freely jointed chain display the same behavior at both large and small forces, although their force–extension curves may disagree by as much as 15% for intermediate forces.

3.5 Buckling

The filaments and sheets of a cell are subject to stress from a variety of sources. For example:

- the membrane and its associated networks may be under tension if the cell has an elevated osmotic pressure,
- components within the cell such as vesicles and filaments experience a variety of forces as they are dragged by molecular motors,
- inequivalent elements of the cytoskeleton may bear differentially the compressive and tensile stresses of a deformation.

As described earlier, such forces in the cell generally have magnitudes in the piconewton range. For a comparison at a macroscopic scale, we calculate the force required to bend a strand of hair. The flexural rigidity κ_f of a solid cylindrical filament of radius R is equal to $\pi YR^4/4$, where Y is the Young's modulus of the material; with $R = 0.05$ mm and $Y = 10^9$ J/m^3 (typical of biomaterials), we expect $\kappa_f = 5 \times 10^{-9}$ J•m for a strand of hair. With one end of a filament of length L held fixed, the free end moves a distance $z = FL^3/(3\kappa_f)$ when subjected to a transverse force F (see end-of-chapter problems). Thus, a force of 1.5×10^5 pN is required to move the free end of a 10 cm strand through a distance of 1 cm. In other words, even this imperceptibly small force on our finger tip is five orders of magnitude larger than the typical force on a filament in the cell.

Newton's Third Law of mechanics tells us that a tensile stress on one component of a cell in equilibrium must be balanced by a compressive stress on another. In the design of bridges and houses, one often sees rigid beams and bars carrying either tension or compression. The simple truss in Fig. 3.12(a) demonstrates how a vertical load is distributed across three beams in a triangle: the two thick elements are under compression while the thin element at the base is subject only to tension. As a design, these

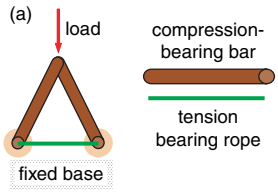

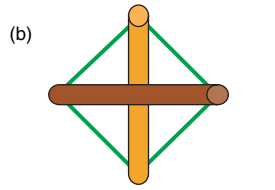

Fig. 3.12

(a) Three elements linked in a triangle bearing a vertical load; two bars are under compression while the rope is under tension. (b) A two-dimensional tensegrity structure of ropes and bars: no two compression-bearing bars are attached.

couplets may make efficient use of materials because a tensile element, in general, needs only a fraction of the cross-sectional area of a compressive element to do its job properly. Space-filling structures built from components that individually bear only tension or only compression include the so-called tensegrities, a two-dimensional example of which is drawn in Fig. 3.12(b). Coined by R. Buckminster Fuller as *tensile-integrity structures* in 1962, tensegrities are intriguing in that rigid compressive elements are often linked only by tension-bearing flexible ropes. The possibility that tensegrities can provide cells with rigidity at an economical cost of materials has been raised by Ingber (see Ingber, 1997, and references therein; Maniotis *et al*., 1997). Certainly, the filaments of the cell do span a remarkable range of bending stiffness – a microtubule is a million times stiffer than a spectrin tetramer – and these filaments may be capable of forming a delicately balanced network if the cell could direct its assembly.

The importance of compression-bearing rods in the cell's architecture depends upon their buckling resistance; in Fig. 3.12(b), the two compressive elements will buckle if the tension sustained by the ropes is too great. Buckling occurs when a force applied longitudinally to a bar exceeds a specific threshold value, which depends upon the length of the bar and its rigidity. We calculate this buckling threshold in two steps. First, we describe the bending of a beam or rod in response to an applied torque (leading to Eq. (3.63)), then we apply this equation to the specific problem of buckling. The calculation follows that of Chapter 38 of Feynmann *et al*. (1964); a more general treatment can be found in Section 21 of Landau and Lifshitz (1986). Readers not interested in the derivation may skip to Eq. (3.69) to see the application to microtubules.

Suppose that we gently bend an otherwise straight bar by applying a torque about its ends. A small segment of the now-curved bar would look something like Fig. 3.13(a), where the top surface of the bar is stretched and the bottom surface is compressed. Near the middle of the bar (depending in part on its cross-sectional shape) lies what is called the neutral surface, within which there is no lateral strain with respect to the original shape. Let's assume that the bend is very gentle and that the neutral surface runs through the midplane of the bar. Measured from the neutral surface, the radius of curvature R is taken to be constant on the small segment in the figure.

The segment has an arc length s along the neutral surface and a length $s + \Delta s$ at a vertical displacement y, where $\Delta s > 0$ when $y > 0$. Because the arcs in Fig. 3.13 have a common center of curvature, then by simple geometry $(s + \Delta s)/s = (R + y)/R$, or

$$\Delta s\,/s = y/R. \tag{3.59}$$

However, $\Delta s\,/s$ is the strain in the longitudinal direction (the strain is the relative change in the length; see Appendix D), telling us that the

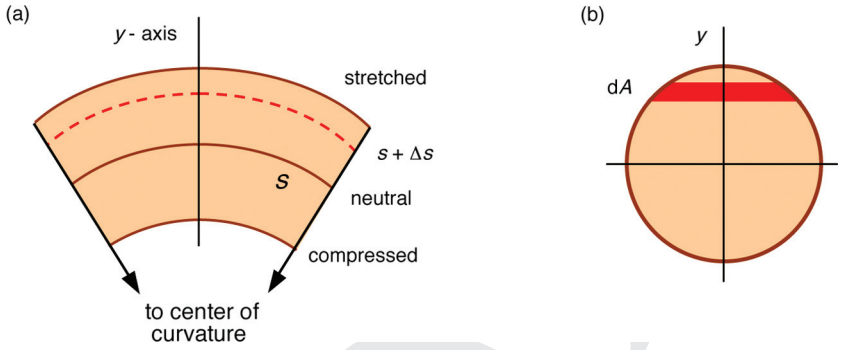

Fig. 3.13

(a) An exaggerated view of a curved rod lying in the plane of the drawing; (b) the (solid) cylindrical rod in cross section. The arc length along the neutral surface is s, which changes to $s + \Delta s$ at a vertical displacement y.

longitudinal strain at y is equal to y/R. The stress that produces this strain is the force per unit area at y, which we write as dF/dA, where dA is the unshaded region at coordinate y in the cross section displayed in Fig. 3.13(b). Stress and strain are related through Young's modulus Y by

$$[stress] = Y\,[strain] \tag{3.60}$$

which becomes $dF/dA = Yy/R$, or

$$dF = (yY/R)\,dA. \tag{3.61}$$

This element of force results in a torque around the mid-plane. Recalling from introductory mechanics that torque is the cross product of force and displacement, the torque must be equal to $y\,dF$, which can be integrated to give the bending moment $\mathcal{M}$:

$$\mathcal{M} = \int y\,dF = (Y/R)\int y^2\,dA, \tag{3.62}$$

after substituting Eq. (3.61) for the force; equivalently

$$\mathcal{M} = Y\mathcal{I}/R. \tag{3.63}$$

The quantity $\mathcal{I}$ made its debut in Section 3.2 as the moment of inertia of the cross section, and has the form

$$\mathcal{I} = \int_{\text{cross section}} y^2\,dA,$$

where the integration is performed only over the cross section of the bar.

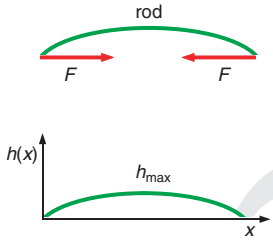

Fig. 3.14

A rod subject to a sufficiently large compressive force F in its longitudinal direction will buckle. The deformed shape can be characterized by a function $h(x)$.

We now apply Eq. (3.63) to the buckling problem, specifically the forces applied to the bar in Fig. 3.14. The coordinate system is defined with $x = 0$ at one end of the bar, whose contour length is L_c. Then, at any given height $h(x)$, the bending moment $\mathcal{M}$ arising from the force F applied to the ends of the bar is equal to

$$\mathcal{M}(x) = Fh(x), \tag{3.64}$$

as expected from the definition of torque ($\mathbf{r} \times \mathbf{F}$). We replace the moment using Eq. (3.63) to obtain

$$Y\mathcal{I}/R(x) = F\,h(x), \tag{3.65}$$

where we emphasize that the radius of curvature R is a function of position by writing it as $R(x)$. From Section 3.2, the radius of curvature at a position $\mathbf{r}$ is defined by $\mathrm{d}^2\mathbf{r}/\mathrm{d}s^2 = \mathbf{n}/R$, where s is the arc length along the curve and $\mathbf{n}$ is a unit normal at $\mathbf{r}$. For gently curved surfaces, $\mathrm{d}^2\mathbf{r}/\mathrm{d}s^2$ can be replaced by $\mathrm{d}^2h/\mathrm{d}x^2$, so that $1/R = -\mathrm{d}^2h/\mathrm{d}x^2$ (the minus sign is needed because $\mathrm{d}^2h/\mathrm{d}x^2$ is negative for our bent rod as drawn). Thus, Eq. (3.65) becomes

$$\mathrm{d}^2h/\mathrm{d}x^2 = -(F/Y\mathcal{I})h(x), \tag{3.66}$$

which is a differential equation for $h(x)$, showing that the second derivative of the height is proportional to the height itself.

From first-year mechanics courses, we recognize this equation as having the same functional form as simple harmonic motion of a spring ($\mathrm{d}^2x/\mathrm{d}t^2 \propto -x(t)$), which we know has a sine or cosine function as its solution. For the specific situation in Fig. 3.14, the solution must be

$$h(x) = h_{\max} \sin(\pi x/L_c), \tag{3.67}$$

where $h_{\max}$ is the maximum displacement of the bend, occurring at $x = L_c/2$ in this approximation. As required, Eq. (3.67) has the property that $h(0) = h(L_c) = 0$. What we are interested in is the allowed range of forces under which buckling will occur, and this can be found by manipulating the solution given by Eq. (3.67). Taking the second derivative of this solution

$$\mathrm{d}^2h/\mathrm{d}x^2 = -(\pi/L_c)^2\, h_{\max} \sin(\pi x/L_c) = -(\pi/L_c)^2 h(x). \tag{3.68}$$

The proportionality constant $(\pi/L_c)^2$ in Eq. (3.68) must be equal to the proportionality constant $F/Y\mathcal{I}$ in Eq. (3.66). This yields

$$F_{\text{buckle}} = \pi^2 Y\mathcal{I}/L_c^2 = \pi^2\kappa_f/L_c^2. \tag{3.69}$$

Now, this expression for the force is independent of $h_{\max}$. What does this mean physically? If the applied force is less than F_{buckle}, the beam will not bend at all, simply compress. However, if $F > F_{\text{buckle}}$, the rod buckles as its ends are driven towards each other. To find out what happens at larger displacements, greater care must be taken with the expression for the curvature. This type of analysis can be applied to the buckling of membranes as well, and has been used to determine the bending rigidity of bilayers (Evans, 1983).

The simple fact that their persistence lengths are comparable to, or less than, cellular dimensions tells us that single actin and spectrin filaments do not behave like rigid rods in the cell. On the other hand, a microtubule appears to be gently curved, because its persistence length is ten to several hundred times the width of a typical cell (see Table 3.2). Can a microtubule

Table 3.2 Linear density λ_p (mass per unit length) and persistence length ξ_p of some biologically important polymers. For the proteins ubiquitin, tenascin and titin, λ_p refers to the unraveled polypeptide.

Polymer	Configuration	λ_p (Da/nm)	ξ_p (nm)
Long alkanes	linear polymer	~110	~0.5
Ubiquitin	linear filament	~300	0.4
Tenascin	linear filament	~300	0.42 ± 0.22
Titin	linear filament	~300	0.4
Procollagen	triple helix	~380	15
Spectrin	two-strand filament	4500	10–20
DNA	double helix	1900	53 ± 2
F-actin	filament	16 000	$(10–20) \times 10^3$
Intermediate filaments	32 strand filament	~50 000	$(0.1–1) \times 10^3$
Tobacco mosaic virus		~140 000	$\sim 1 \times 10^6$
Microtubules	13 protofilaments	160 000	$4–6 \times 10^6$

withstand the typical forces in a cell without buckling? Taking its persistence length ξ_p to be 3 mm, in the mid-range of experimental observation, the flexural rigidity of a microtubule is $\kappa_f = k_B T \xi_p = 1.2 \times 10^{-23}$ J•m. Assuming 5 pN to be a commonly available force in the cell, Eq. (3.69) tells us that a microtubule will buckle if its length exceeds about 5 μm, not a very long filament compared to the width of some cells. If 10–20 μm long microtubules were required to withstand compressive forces in excess of 5 pN, they would have to be bundled to provide extra rigidity, as they are in flagella.

Both of these expectations for the bucking of microtubules have been observed experimentally (Elbaum *et al.*, 1996). When a single microtubule of sufficient length resides within a floppy phospholipid vesicle, the vesicle has the appearance of an American football, whose pointed ends demarcate the ends of the filament. As tension is applied to the membrane by means of aspirating the vesicle, the microtubule ultimately buckles and the vesicle appears spherical. In a specific experiment, a microtubule of length 9.2 μm buckled at a force of 10 pN, consistent with our estimates above. When a long bundle of microtubules was present in the vesicle, the external appearance of the vesicle resembled the Greek letter ϕ, with the diagonal stroke representing the rigid bundle and the circle representing the bilayer of the vesicle. In other words, although they are not far from their buckling point, microtubules are capable of forming tension–compression couplets with membranes or other filaments. However, more

flexible filaments such as actin and spectrin are most likely restricted to be tension-bearing elements.

3.6 Measurements of bending resistance

The bending deformation energy of a filament can be characterized by its flexural rigidity κ_f. Having units of [*energy* • *length*], the flexural rigidity of uniform rods can be written as a product of the Young's modulus Y (units of [*energy* • *length*^{3}]) and the moment of inertia of the cross section $\mathcal{I}$ (units of [*length*^{4}]): $\kappa_f = Y\mathcal{I}$. At finite temperature T, the rod's shape fluctuates, with the local orientation of the rod changing strongly over length scales characterized by the persistence length $\xi_p = \kappa_f / k_B T$, where k_B is Boltzmann's constant. We now review the experimental measurements of κ_f or ξ_p for a number of biological filaments, and then interpret them using results from Sections 3.2–3.5.

3.6.1 Measurements of persistence length

Mechanical properties of the principal structural filaments of the cytoskeleton – spectrin, actin, intermediate filaments and microtubules – have been obtained through a variety of methods. In first determining the persistence length of spectrin, Stokke *et al*. (1985a) related the intrinsic viscosity of a spectrin dimer to its root-mean-square radius, from which the persistence length could be extracted via a relationship like Eq. (3.33). The resulting values of ξ_p covered a range of 15–25 nm, depending upon temperature. Another approach (Svoboda *et al*., 1992) employed optical tweezers to hold a complete erythrocyte cytoskeleton in a flow chamber while the appearance of the cytoskeleton was observed as a function of the salt concentration of the medium. It was found that a persistence length of 10 nm is consistent with the measured mean squared end-to-end displacement $\langle r_{ee}^2 \rangle$ of the spectrin tetramer and with the dependence of the skeleton's diameter on salt concentration. Both measurements comfortably exceed the lower bound of 2.5 nm placed on the persistence length of a spectrin *monomer* (as opposed to the intertwined helix in the cytoskeleton) by viewing it as a freely jointed chain of segment length $b = 5$ nm and invoking $\xi_p = b/2$ from Eq. (3.34) (5 nm is the approximate length of each of approximately 20 barrel-like subunits in a spectrin monomer of contour length 100 nm; see Fig. 3.1(a)).

The persistence length of F-actin has been extracted from the analysis of more than a dozen experiments, although we cite here only a few works as an introduction to the literature. The measurements involve both native and

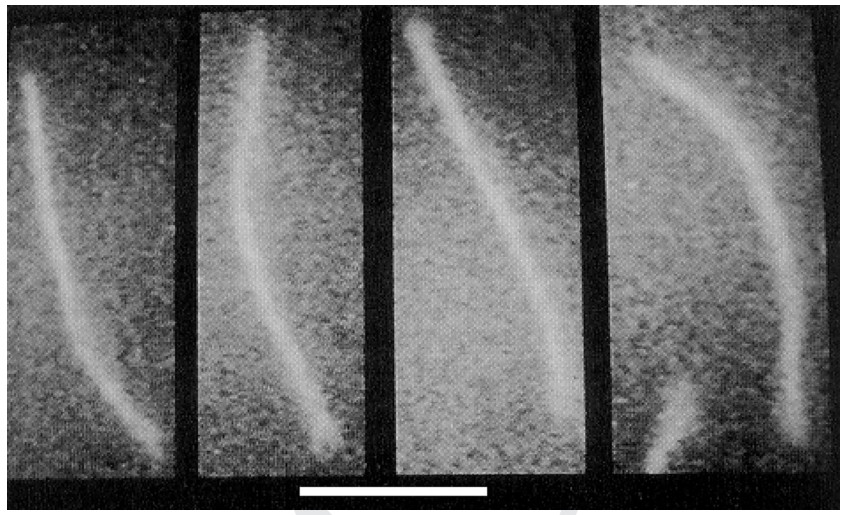

Fig. 3.15 Thermal fluctuations of a rhodamine-labeled actin filament observed by fluorescence microscopy at intervals of 6 s (bar is 5 μm in length; reprinted with permission from Isambert *et al.*, 1995; ©1995 by the American Society for Biochemistry and Molecular Biology).

fluorescently labeled actin filaments, which may account for some of the variation in the reported values of ξ_p. The principal techniques include:

(i) dynamic light scattering, which has given a rather broad range of results, converging on $\xi_p \sim 16$ μm (Janmey *et al.*, 1994);
(ii) direct microscopic observation of the thermal fluctuations of fluorescently labeled actin filaments, as illustrated in Fig. 3.15. Actin filaments stabilized by phalloidin are observed to have $\xi_p = 17$–19 μm (Gittes *et al.*, 1993; Isambert *et al.*, 1995; Brangwynne *et al.*, 2007), while unstabilized actin filaments are more flexible, at $\xi_p = 9 \pm 0.5$ μm (Isambert *et al.*, 1995);
(iii) direct microscopic observation of the driven oscillation of labeled actin filaments give $\xi_p = 7.4 \pm 0.2$ μm (Riveline *et al.*, 1997).

Taken together, these experiments and others indicate that the persistence length of F-actin lies in the 10–20 μm range, about a thousand times larger than spectrin dimers.

Microtubules have been measured with several of the same techniques as employed for extracting the persistence length of actin filaments. Again, both pure and treated (in this case, taxol-stabilized) microtubules have been examined by means of:

(i) direct microscopic observation of the bending of microtubules as they move within a fluid medium, yielding ξ_p in the range of 1–8 mm (Venier *et al.*, 1994; Kurz and Williams, 1995; Felgner *et al.*, 1996);

(ii) direct microscopic observation of the thermal fluctuations of microtubules. Most measurements (Gittes *et al.*, 1993; Venier *et al.*, 1994; Kurz and Williams, 1995; Brangwynne *et al.*, 2007) give a range of 1–6 mm, and up to 15 mm in the presence of stabilizing agents (Mickey and Howard, 1995). More recent work which examines the dependence of ξ_p on the microtubule growth rate confirms the 4–6 mm range (Janson and Dogterom, 2004);

(iii) direct microscopic observation of the buckling of a single, long microtubule confined within a vesicle under controlled conditions, leading to $\xi_p = 6.3$ mm (Elbaum *et al.*, 1996), although one experiment gives notably lower values (Kikumoto *et al.*, 2006).

Thus, the persistence length of microtubules is more than an order of magnitude larger than a typical cell diameter, with many measurements concentrated in the 4–6 mm range. Some experiments have reported that the flexural rigidities of microtubules appears to depend on the length of the filament (Kis *et al.*, 2002; Pampaloni, 2006), a situation that can arise when the shear modulus of a filament is much lower than its longitudinal Young's modulus (Li *et al.*, 2006a).

The filaments of the cytoskeleton are not the only polymers whose mechanical properties are important to the operation of the cell. For example, the packing of DNA into the restricted volume of the cell is a significant challenge, given both the contour length and persistence length of a DNA molecule. Measurements of the DNA persistence length date back at least two decades to the work of Taylor and Hagerman (1990), who found $\xi_p = 45 \pm 1.5$ nm by observing the rate at which a linear strand of DNA closes into a circle. Other experiments directly manipulate a single DNA molecule by attaching a magnetic bead to one end of the filament (while the other is held fixed) and applying a force by means of an external magnetic field. The resulting force–extension relation for DNA from bacteriophage lambda (a virus that attacks bacteria such as *E. coli*) is found to be well-described by the worm-like chain model, Eq. (3.58), which involves only two parameters – the contour length and the persistence length (Bustamante *et al.*, 1994). As well as yielding a fitted contour length in agreement with the crystallographic value, the procedure gives a fitted persistence length of 53 ± 2 nm, in the same range as found earlier by Taylor and Hagerman. Yet another approach records the motion of a fluorescently labeled DNA molecule in a fluid (Perkins *et al.*, 1995), the analysis of which gives $\xi_p \sim 68$ nm (Stigter and Bustamante, 1998), a slightly higher value than that of unlabelled DNA. The torsion resistance of DNA is described in Section 4.3; note that ξ_p may depend strongly on experimental conditions (see, for example, Amit *et al.*, 2003).

The above measurements are summarized in Table 3.2, which also displays the mass per unit length of the filament (from Section 3.1). For

comparison, the table includes very flexible alkanes (from Flory, 1969) as well as the proteins procollagen (Sun *et al.*, 2002), tenascin (Oberhauser *et al.*, 1998), titin (Rief *et al.*, 1997) and ubiquitin (Chyan *et al.*, 2004). Single chains of the polysaccharide cellulose exhibit a range of persistence lengths of 5–10 nm, depending on conditions (Muroga *et al.*, 1987). The tobacco mosaic virus is a hollow rod-like structure with a linear density similar to that of a microtubule and a persistence length to match. Experimentally, the flexural rigidity of the virus on a substrate is obtained by observing the response of the virus when probed by the tip of an atomic force microscope (Falvo *et al.*, 1997). The persistence lengths of intermediate filaments are less well understood, with ξ_p of desmin lying in the range 0.1 to 1 μm as measured by dynamic light scattering (Hohenadl *et al.*, 1999). In this case and several others, the persistence length quoted in Table 3.2 is found from the flexural rigidity via Eq. (3.21). The persistence length of fibrin protofilaments with a radius of 10 nm has been measured to be 0.5 μm (Storm *et al.*, 2005).

3.6.2 ξ_p and Young's modulus

The measured persistence lengths in Table 3.2 span more than six orders of magnitude, a much larger range than the linear density, which covers about three orders of magnitude. We can understand this behavior by viewing the polymers as flexible rods, whose flexural rigidity from Eq. (3.2) is

$$\kappa_f = Y\mathcal{I}, \tag{3.70}$$

and whose corresponding persistence length, according to Eq. (3.21), is

$$\xi_p = Y\mathcal{I} / k_B T, \tag{3.71}$$

where the moment of inertia of the cross section for hollow rods of inner radius R_i and outer radius R is (from Eq. (3.13))

$$\mathcal{I} = \pi(R^4 - R_i^4)/4.$$

For some hollow biofilaments like the tobacco mosaic virus, for which $R/R_i \sim 4.5$, only a small error is introduced by neglecting R_i^4 in the expression for $\mathcal{I}$, so that

$$\xi_p \cong \pi Y R^4 / 4k_B T, \tag{3.72}$$

although we note that this expression is in error by a factor of two for microtubules ($R \sim 14$ nm and $R_i \sim 11.5$ nm; see Amos and Amos, 1991). Being raised to the fourth power, R must be known relatively well to make an accurate prediction with Eq. (3.72). Such is not always the case, and a somewhat gentler approach which, in some sense averages over the bumpy atomic boundary of a molecule, replaces R^2 by the mass per unit length λ_p

using the relationship $\lambda_p = \rho_m \pi R^2$ for a cylinder, where ρ_m is the mass per unit volume. Thus, we obtain

$$\xi_p \cong (Y / 4\pi k_B T \rho_m^2)\, \lambda_p^2, \tag{3.73}$$

which implies that the persistence length should be proportional to the square of the mass per unit length, if Y and ρ_m are relatively constant from one filament to the next.

Data from Table 3.2 are plotted logarithmically in Fig. 3.16 as a test of the quadratic dependence of ξ_p on λ_p suggested by Eq. (3.73). With the exception of spectrin, which is a loosely intertwined pair of filaments, the data are consistent with the fitted functional form $\xi_p = 2.5 \times 10^{-5}\, \lambda_p^2$, where ξ_p is in nm and λ_p is in Da/nm. Because the data span so many orders of magnitude, the approximations (such as constant Y and ρ_m) behind the scaling law are supportable, and the graph can be used to find the Young's modulus of a generic biofilament. Equating the fitted numerical factor 2.5×10^{-5} nm^3/Da^2 with $Y / 4\pi k_B T \rho_m^2$ gives $Y = 0.5 \times 10^9$ J/m^3 for $k_B T = 4 \times 10^{-21}$ J and $\rho_m = 10^3$ kg/m^3 (which is the density of water, or roughly the density of many hydrocarbons). Although no more accurate than a factor of two, this value of Y is in the same range as $Y = 1$–2×10^9 J/m^3 found for collagen (linear density of 1000 Da/nm; for collagen fibrils, see Shen *et al.*, 2008), but much smaller than that of dry cellulose (8×10^{10} J/m^3) or steel (2×10^{11} J/m^3). Of course, Eq. (3.73) can be applied to individual filaments if their radii and persistence lengths are sufficiently well known, yielding $Y \sim (0.5$–$1.5) \times 10^9$ J/m^3 for most filaments. An analysis of the indentation of microtubules using an AFM tip yields 0.6×10^9 J/m^3 (Schaap *et al.*, 2006). Note that the Young's modulus of individual

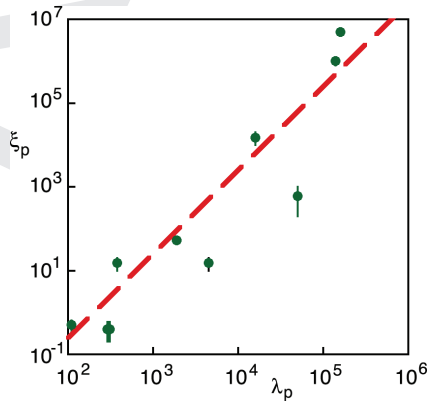

Fig. 3.16 Logarithmic plot of persistence length ξ_p against linear density λ_p for the data in Table 3.2. The straight line through the data is the function $\xi_p = 2.5 \times 10^{-5}\, \lambda_p^2$, where ξ_p is in nm and λ_p is in Da/nm.

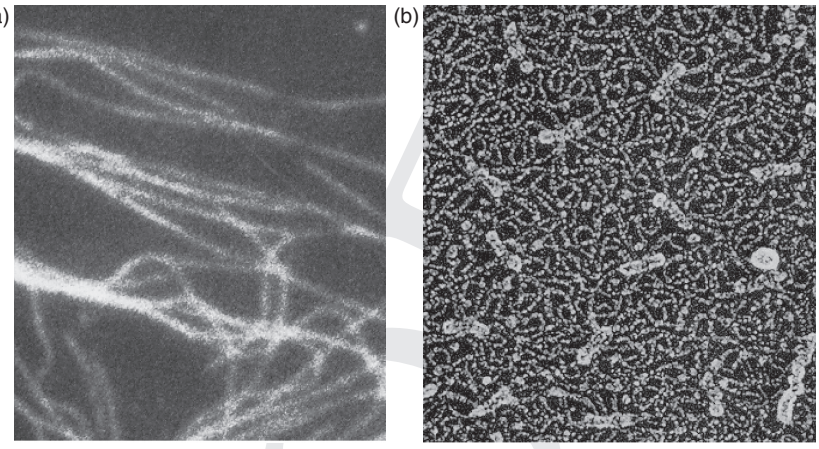

Fig. 3.17 (a) Microtubules, with a persistence length in the millimeter range, are relatively stiff on cellular length scales (image is about 10 μm across, reprinted with permission from Osborn *et al*., 1978; ©1978 by the Rockefeller University Press), in contrast to spectrin (b), which has a persistence length five orders of magnitude smaller as seen in the human erythrocyte (distance between actin nuggets is about 100 nm; reprinted with permission from Coleman *et al*. 1989; ©1989 by Wiley-Liss; image prepared by John Heuser, Washington University; see also Heuser, 1983).

filaments may be strongly hydration dependent; for example, intermediate filaments from hagfish slime possess a Young's modulus that drops from 3.6×10^9 J/m^3 when dry to just 0.006×10^9 J/m^3 when hydrated (Fudge and Gosline, 2004). The decrease of Y upon hydration of a filament is observed for collagen fibrils as well (van der Rijt *et al*., 2006).

3.6.3 Filament configurations in the cell

Knowing their flexural rigidities, how do we expect cytoskeletal filaments to behave in the cell? As one representative situation, we examine microtubules, which can easily be as long as a typical cell is wide (say 10 μm) and have a persistence length one hundred times the cell diameter. Microtubules should not display very strong thermal oscillations, and indeed Eq. (3.20) demonstrates that the root mean square angle of oscillation $\langle \theta^2 \rangle^{1/2}$ is about a tenth of a radian (or about 6°) for a sample microtubule with $L_c = 10$ μm if the persistence length is in the mid-range of the experimental values, say $\xi_p = 2 \times 10^3$ μm. This doesn't mean that microtubules in the cell behave quite like steel rods in a plastic bag, as can be seen by the image in Fig. 3.17(a), but a generous amount of energy is required to give our sample microtubule a substantial curvature: for example, Eq. (3.10) for E_{arc} becomes $E_{arc} = (\xi_p / 2L_c)\, k_B T$ when $R_c = L_c$, and this yields $E_{arc} = 100\, k_B T$ for $R_c = L_c =$

10 μm. Indeed, Elbaum *et al*. (1996) observe that a single microtubule with a length longer than the mean diameter of an artificial vesicle can cause the vesicle to deform into an ovoid.

Having a persistence length about one-tenth of its contour length, a spectrin tetramer should appear contorted on cellular length scales. In fact, its mean end-to-end displacement $\langle r_{ee}^2 \rangle^{1/2}$ is just 75 nm, which is only one-third of its contour length (200 nm), so the tetramers form a sinuous web when joined to form a network, as shown in Fig. 3.17(b). Thus, the network of spectrin tetramers in the human erythrocyte cytoskeleton can be stretched considerably to achieve a maximum area that is $(200/75)^2 \sim 7$ times its equilibrium area. As discussed in Section 3.4, highly convoluted chains such as spectrin resist extension, behaving like entropic springs with a spring constant $k_{sp} = 3k_B T / 2\xi_p L_c$ in three dimensions, from Eq. (3.54). Our spectrin tetramer, then, has a spring constant of about 2×10^{-6} J/m^2, which, although not a huge number, helps provide the cytoskeleton with enough shear resistance to restore a red cell to its equilibrium shape after passage through a narrow capillary. Lastly, we recall from the definition $\xi_p = \kappa_f / k_B T$ that the persistence length should decrease with temperature, if the flexural rigidity is temperature-independent. The temperature-dependence of the elasticity of biofilaments has not been as extensively studied as that of conventional polymers, but Stokke *et al*. (1985a) do find that the persistence length decreases with temperature roughly as expected for an entropic spring.

3.6.4 Filamentous cells

Many genera of cells form long filaments whose appearance ranges from beads on a string to relatively rigid rods. Two examples from the world of cyanobacteria are displayed in Fig. 2.1. The mechanical deformation of these filaments can be analyzed within the same formalism introduced earlier in this chapter: each filament possesses an intrinsic resistance to bending, twisting, etc. Yet there are few direct measurements of filament elasticity based on conventional stress–strain curves, in which the deformation of a filament is observed in response to a known applied stress. Further, the thermal fluctuations in overall filament shape are relatively tiny compared to what they are on a molecular level (see end-of-chapter problems), eliminating this approach as an appropriate technique for extracting elastic parameters. However, the scaling behavior of the flexural rigidity can be probed by constructing a tangent correlation function for randomly stirred filaments in a fluid, and one finds that κ_f increases like R^4 or perhaps R^3 with increasing filament radius R for filamentous cyanobacteria within a given genus.

Summary

Sometimes criss-crossing the interior of a cell, sometimes forming a mat or wall around it, the biological chains and filaments of the cell range in diameter up to 25 nm and have a mass per unit length covering more than three orders of magnitude, from ~100 Da/nm for alkanes to 160 kDa/nm for microtubules. A simple mathematical representation of these filaments views them as structureless lines characterized by a position $\mathbf{r}(s)$ and tangent vector $\mathbf{t}(s) = \partial\mathbf{r}(s)/\partial s$, where s is the arc length along the line. The lowest order expression for the energy per unit length of deforming a filament from its straight-line configuration is $(\kappa_f/2)(\partial\mathbf{t}(s)/\partial s)^2$, where κ_f is the flexural rigidity of the filament.

At non-zero temperature, filaments can exchange energy with their surroundings, permitting their shapes to fluctuate as they bend and twist. Their orientation changes direction with both position and time, such that the direction of the tangent vectors to the filament decays as $\langle \mathbf{t}(0) \cdot \mathbf{t}(s) \rangle = \exp(-s/\xi_p)$ due to thermal motion, where the persistence length $\xi_p = \kappa_f / k_B T$ depends upon the temperature T (k_B is Boltzmann's constant). Also, because of fluctuations, the squared end-to-end displacement $\mathbf{r}_{ee}$ of a filament is less than its contour length L_c, having the form $\langle r_{ee}^2 \rangle = 2\xi_p L_c - 2\xi_p^2 [1 - \exp(-L_c/\xi_p)]$, which approaches the rigid rod limit $\langle r_{ee}^2 \rangle^{1/2} \sim L_c$ only when $\xi_p >> L_c$. In comparison, long filaments with relatively short persistence lengths obey the form $\langle r_{ee}^2 \rangle = 2\xi_p L_c$, showing that the linear size of sinuous filaments grows only like the square root of the contour length, a property of all linear chains in which self-avoidance is neglected. When self-avoidance is enforced, the exponent n in the scaling relation $\langle r_{ee}^2 \rangle^{1/2} \propto L_c^n$ is dimension-dependent, achieving ideal behavior $n = 1/2$ only in four dimensions. Branched polymers or linear chains with attractive interactions display still different scaling behavior.

At finite temperature, $\mathbf{r}_{ee}$ does not have a unique value but rather is distributed according to a probability per unit length of the form $\mathcal{P}(x) = (2\pi\sigma^2)^{-1/2} \exp(-x^2 / 2\sigma^2)$ for filaments in one dimension, where x is the displacement from one end of the polymer chain to the other. For freely jointed chains with N identical segments of length b, the variance is given by $\sigma^2 = Nb^2/d$, where d is the spatial dimension of the chain. This distribution demonstrates that a chain is not likely to be found in its fully stretched configuration $r_{ee} = L_c$ because such a configuration is strongly disfavored by entropy. Thus, the free energy of a flexible chain rises as the chain is stretched from its equilibrium value of r_{ee}, and the chain behaves like an entropic spring with a force constant $k_{sp} = 3k_B T / 2\xi_p L_c = 3k_B T / \langle r_{ee}^2 \rangle$ in three dimensions. The ideal spring behavior $f = k_{sp} x$ is valid only at small extensions and the probability distribution function $\mathcal{P}(x)$ does not take into account the fact

that $\mathcal{P}(x>L_c) = 0$: the end-to-end displacement of the chain cannot exceed its contour length. As the chain becomes increasingly stretched, the relation between applied force and extension is much better described by the worm-like chain model, where $\xi_p f / k_B T = (2(1 - x/L_c))^{-2} - 1/4 + x/L_c$.

The persistence lengths of a variety of the cell's polymers and filaments have been measured, and they span the enormous range of 0.5 nm for alkanes up to a few millimeters for microtubules. This behavior can be understood by viewing the filament as a flexible rod of uniform density and cross section, permitting the flexural rigidity to be written as $\kappa_f = Y\mathcal{I}$, where Y is the material's Young's modulus. The moment of inertia of the cross section $\mathcal{I}$ has the form $\mathcal{I} = \pi(R^4 - R_i^4)/4$ for a hollow tube of inner and outer radii R_i and R, respectively, predicting that the persistence length has the form $\xi_p = \pi Y(R^4 - R_i^4) / 4k_B T$. Treated as uniform rods, the filaments of the cell have Young's moduli in the range $(0.5 - 1.5) \times 10^9$ J/m^3, which is about two orders of magnitude lower than the moduli of conventionally "hard" materials such as wood or steel, but comparable to plastics.

Problems

Applications

3.1. The interiors of some cylindrically shaped bacteria are known to contain filaments that wind around the inside of the membrane, adopting the shape of a helix as they travel along the cylindrical part of the bacterium. Suppose the filament advances 3 μm along the cylinder while it executes one complete turn, for a cylinder of diameter 1 μm.

(a) What is the length of this section of the filament?
(b) What angle α does it make with respect to a plane perpendicular to the cylindrical axis?

3.2. Consider a large motor neuron running from the brain to the arm containing a core bundle of microtubules. Taking the persistence length of a microtubule to be 2 mm, what energy is required (in $k_B T$ at 300 K) to bend a microtubule of length 20 cm into an arc of radius 10 cm?

3.3. Let θ be the angle characterizing the change in direction of a filament along its length. For a tobacco mosaic virus of contour length 250 nm, determine the value of $\langle \theta^2 \rangle^{1/2}$ arising from thermal fluctuations. Quote your answer in degrees.

3.4. Consider a piece of spaghetti 2 mm in diameter. If the Young's modulus Y of this material is 1×10^8 J/m^3, what is the persistence length of

the spaghetti at $T = 300$ K? Is the result consistent with your everyday observations?

3.5. Flagella are whip-like structures typically about 10 μm long whose bending resistance arises from a microtubule core. Treating the flagellum as a hollow rod of inner radius 0.07 μm and outer radius 0.1 μm, find its persistence length at $T = 300$ K if its Young's modulus is 1×10^8 J/m^3. Compare your result with the persistence length of a single microtubule. (*Note: this approximation is not especially trustworthy*.)

3.6. What are the structural advantages for a microtubule to be hollow? Calculate the mass ratio and the flexural rigidity ratio for a hollow microtubule with inner and outer radii 11.5 nm and 14 nm, respectively, compared to a solid microtubule with the same outer radius. What is the most efficient use of construction materials such as proteins to gain rigidity: one solid microtubule or several hollow ones?

3.7. The virus bacteriophage-λ contains a string of 97 000 base pairs in its DNA. (a) Find the contour length of this DNA strand at 0.34 nm/base-pair and compare it with the DNA persistence length. (b) If the DNA is 2 nm in diameter, what is the radius of the smallest spherical volume into which it can be packed? (c) If this DNA becomes a random chain once released into a host cell, what is its root mean square end-to-end displacement? Compare your answers to parts (b) and (c) with the size of a typical bacterium.

3.8. (a) Compare the root mean square end-to-end distance $\langle r_{ee}^2 \rangle^{1/2}$ of strands of spectrin, actin and microtubules 200 nm in contour length, using both the exact and approximate expressions from Section 3.3. Comment on the difference between the results. (b) What is the effective spring constant (in N/m) in three dimensions for each type of protein, for filaments with a contour length of 1 cm at 300 K? Use $\xi_p = 15$, 15×10^3, and 2×10^6 nm for spectrin, actin and microtubules, respectively.

3.9. Consider a 30 μm length of DNA, such as might be found in a virus. What force is required to stretch the DNA to an end-to-end displacement $x = 10$, 20 and 25 μm, according to (a) the Gaussian approximation and (b) the worm-like chain model of Section 3.4? Quote your answer in N, and assume the temperature is 300 K. Comment on the accuracy of the Gaussian approximation.

3.10. Eukaryotic cells package their DNA by wrapping short stretches of it around the rims of disk-shaped proteins called histones. In a typical situation, a 150 base-pair segment of DNA wraps itself 1.7 times around the histone core. (a) What is the curvature of the DNA? (b) What is the bending energy (in units of $k_B T$) associated with this deformation if the DNA persistence length is 53 nm?

3.11. Compare the two force–extension relations in Eqs. (3.55) and (3.58) by plotting $\xi_p f / k_B T$ against x / L_c. At what value of x / L_c is the difference between these curves the largest?

3.12. *Oscillatoria* is a genus of filamentous cyanobacteria that execute slow side-to-side movement with a typical angular range of $\langle \theta^2 \rangle^{1/2} \sim 0.1$. For the sake of illustration, take the length and diameter of an *Oscillatoria* filament to be 100 μm and 5 μm respectively, and its Young's modulus to be 10^9 J/m^3. (a) Determine $\langle \theta^2 \rangle^{1/2}$ arising from thermal oscillations and compare your result to the observed variation. (b) Find the buckling force applicable to this specimen.

3.13. One end of a microtubule of length $L = 5$ μm is subject to a lateral force of 0.5 pN while the other end is held fixed. Assuming this filament to have a persistence length ξ_p of 2 mm at room temperature, do the following.

(a) Find the lateral displacement z of the free end of the microtubule; use the result from Problem 3.31 without proof and quote your answer in μm.
(b) Estimate the angular displacement θ of the free end by using z from part (a).
(c) Compare this result with $\langle \theta^2 \rangle^{1/2}$ from thermal fluctuations.

3.14. In a hypothetical system, two parallel plates are linked by a large number of identical polymer chains in parallel with each other. The polymers have a length of 50 nm and a persistence length of 0.5 nm.

(a) What is the entropic spring constant for each polymer at a temperature of $T = 300$ K. Quote your answer in N/m.
(b) If the polymers uniformly cover an area of 1 cm^2 on each plate, how many of them are required to generate a macroscopic spring constant of 10^7 N/m between the plates?
(c) What is the rough spacing between polymers in part (b)? For simplicity, assume that they are arranged in a square pattern on each plate. Quote your answer in nm and compare it with the contour length of the polymer.

3.15. Find the ratio of the flexural rigidities of the mast and rigging of an old sailboat. Use the following values for Young's modulus Y and diameter of the components:

- mast: $Y = 10^{10}$ J/m^3, diameter = 30 cm,
- ropes: $Y = 2 \times 10^9$ J/m^3, diameter = 5 cm.

Compare this ratio to that for microtubules and actin, using data from Table 3.2.

Formal development and extensions

Some of the following problems require definite integrals for their solution.

$$\int_0^\infty \exp(-x^2)\,dx = \sqrt{\pi}/2 \qquad \int_0^\infty x^2 \exp(-x^2)\,dx = \sqrt{\pi}/4$$

$$\int_0^\infty x^3 \exp(-x^2)\,dx = 1/2 \qquad \int_0^\infty x^4 \exp(-x^2)\,dx = 3\sqrt{\pi}/8$$

3.16. The curvature $C(s)$ of a particular deformed filament of contour length L is described by the function $C(s) = C_o s/L$, where s is the arc length along the filament.

(a) Draw the shape of the filament over the range $0 \le s \le L$ when $C_o = 1/L$.
(b) For a flexural rigidity κ_f, what is the bending energy of the deformation?

3.17. The path of a uniform helix is described by the Cartesian coordinates:

$$x(s) = a\cos(2\pi s/s_o)$$
$$y(s) = a\sin(2\pi s/s_o)$$
$$z(s) = ps/s_o,$$

where s is the arc length, $s_o = (p^2 + (2\pi a)^2)^{1/2}$, and the parameters a and p have the dimensions of length (the radius and pitch of the helix, respectively).

(a) Find the unit tangent vector and unit normal vector to the curve at arbitrary s.
(b) Obtain an expression for the local curvature C.
(c) Find the behavior of C in the two limits $a >> p$ and $a << p$; interpret your results.

3.18. Show that the curvature C of the trajectory of a particle moving with velocity $\mathbf{v}$ and acceleration $\mathbf{a}$ can be found from the cross product $|\mathbf{v} \times \mathbf{a}| = Cv^3$.

3.19. Consider a polymer such as a linear alkane, where the bond angle between successive carbon atoms is a fixed value α, although the bonds are free to rotate around one another.

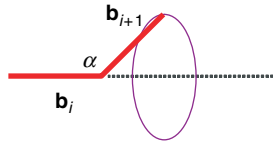

The length and orientation of the bond between atom i and atom $i+1$ defines a bond vector $\mathbf{b}_i$. Assume all bond lengths are the same, and that remote bonds can intersect.

(a) Show that the average projection of $\mathbf{b}_{i+k}$ on $\mathbf{b}_i$ is

$$\langle \mathbf{b}_i \bullet \mathbf{b}_{i+k} \rangle = b^2(-\cos\alpha)^k. \qquad (k \geq 0)$$

[*Hint: start with* $\langle \mathbf{b}_i \bullet \mathbf{b}_{i+1} \rangle$ *and iterate*.]

(b) Write $\langle \mathbf{r}_{ee}^2 \rangle$ in terms of $\langle \mathbf{b}_i \bullet \mathbf{b}_j \rangle$ to obtain

$$\langle \mathbf{r}_{ee}^2 \rangle / b^2 = N\,[1 + (2–2/N)(-\cos\alpha) + (2–4/N)(-\cos\alpha)^2 + \ldots].$$

(c) Use your result from (b) to establish that, in the large N limit

$$\langle \mathbf{r}_{ee}^2 \rangle = Nb^2\,(1 - \cos\alpha) / (1 + \cos\alpha).$$

(d) What is the effective bond length (in units of b) in this model at the tetrahedral value of 109.5°?

3.20. The backbones of polymers such as the polysiloxanes have alternating unequal bond angles, even though the bond lengths are all equal.

(a) Show that, if self-intersections of this type of chain are permitted, its effective bond length is $B_{eff}^2 = b^2\,(1 - \cos\alpha) \bullet (1 - \cos\beta)\,/\,(1 - \cos\alpha\cos\beta)$. [*Hint: follow the same steps as in Problem 3.19*.]

(b) Confirm that this expression reduces to the fixed-angle rotating chain expression in Problem 3.19(c) when $\alpha = \beta$.

(c) Evaluate B_{eff} when $\alpha = 109.5°$, $\beta = 130°$ and $b = 0.17$ nm.

3.21. Show that $\langle |\mathbf{r}_{ee}| \rangle = (8/3\pi)^{1/2} N^{1/2} b$ for ideal chains in three dimensions.

3.22. The radius of gyration, or root mean square radius, R_g of the N+1 vertices in a linear chain, is defined by

$$R_g^2 = [\Sigma_{i=1,N+1}\,(\mathbf{r}_i - \mathbf{r}_{cm})^2]\,/\,(N+1),$$

where $\mathbf{r}_i$ is the position vector of each of the N+1 vertices and $\mathbf{r}_{cm}$ is the center-of-mass position $\mathbf{r}_{cm} = \Sigma_i \mathbf{r}_i\,/\,(N+1)$. Show that $\langle R_g^2 \rangle = \langle r_{ee}^2 \rangle / 6$ for ideal chains. [*Hint: recast the problem to read* $R_g^2 \propto \Sigma\Sigma\, r_{ij}^2$ *and then use* $\langle r_{ij}^2 \rangle = |j - i| b^2$ *where* $\mathbf{r}_{ij}$ *is the displacement between vertices i and j. Justify!]*

3.23. Find $r_{ee,\,\text{most likely}}$ and $\langle |\mathbf{r}_{ee}| \rangle$ for ideal chains in two dimensions.

3.24. Suppose that a particle moves only in one direction at a constant speed v but changes direction randomly at the end of every time interval Δt.

(a) Find the diffusion coefficient D of the motion as a function of v and Δt, given the diffusion equation $\langle x^2 \rangle = 2Dt$.
(b) Find the temperature dependence of D if the kinetic energy of the particle is $k_B T/2$.

3.25. Consider a three-dimensional ideal chain of 50 segments, each with length 10 nm.

(a) What are $\langle |\mathbf{r}_{ee}| \rangle$ and $\langle \mathbf{r}_{ee}^2 \rangle^{1/2}$?
(b) What is the effective spring constant (in N/m) at 300 K?
(c) If the chain has charges +/–e on each end and is placed in a field of 10^6 V/m, what is the change in the end-to-end distance?

3.26. The results in the text for the distribution of $\mathbf{r}_{ee}$ for random chains in three dimensions can be generalized easily to random chains in d dimensions. For chains whose N segments have a uniform length b, show that:

(a) the distribution of end-to-end distances has the conventional Gaussian form, but with $\sigma_d^2 = Nb^2/d$,
(b) the effective spring constant is $k_{sp} = dk_B T / Nb^2$.

3.27. Show that the flexural rigidity κ_f of a solid beam having a rectangular cross section of width w and thickness t is given by $\kappa_f = Ywt^3/12$, where the axis of the bending deformation is through the center of the rectangle as shown.

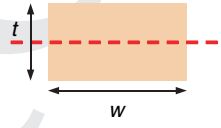

3.28. Consider a hollow rod with the cross section of a square as shown, where the length of a side is a and the thickness is t. Determine the moment of inertia of the cross section of this shape in the limit where $t << a$. Place the axis of the bending motion through the center of the square.

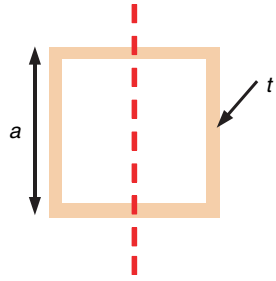

3.29. Determine the moment of inertia of the cross section $\mathcal{I}$ for the three regular-shaped rods with cross sections (S_1, S_2, H) as shown (the dashed line indicates the axis around which the rod is to bend).

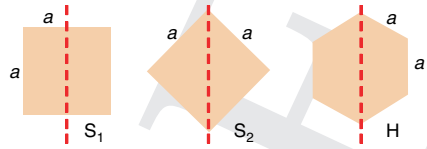

Take the length of all sides to be a. Find the ratio of these moments to that of a cylinder of radius R ($\mathcal{I} = \pi R^4/4$), imposing the condition that all shapes have the same cross-sectional area πR^2 to express a in terms of R.

3.30. Two uniform cylindrical rods, each of radius R, are joined side by side as shown. What is the moment of inertia of the cross section $\mathcal{I}$ of the combined pair? Compared to the flexural rigidity of a single rod (with a bending axis through its center), what is the rigidity of the pair? You may NOT use the parallel axis theorem.

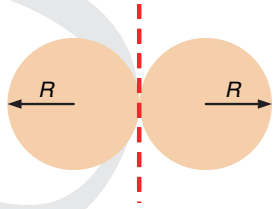

3.31. A massless rod of length L lies horizontally with one end free and one end held so that it can neither translate nor rotate. A force F is applied in the upward direction to the free end.

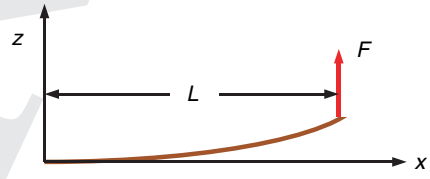

For gentle bends, show that the displacement $z(x)$ of the rod at any horizontal position x is given by

$$z(x) = (F / Y\mathcal{I}) \bullet (Lx^2/2 - x^3/6),$$

where Y and $\mathcal{I}$ are the beam's Young's modulus and moment of inertia of the cross section. What is the displacement of the rod at $x = L$? [*Hint: find the analog of Eq. (3.65) for a force perpendicular to the filament; after Chapter 38 of Feynmann et al.*, 1964].